Pre-Clinical Assessment of MCL-1 as a Therapeutic Target in T-Cell Lymphomas

Pre-clinical assessment of MCL-1 as a therapeutic target in T-cell lymphomas

Amanda L. Christie

A Thesis in the Field of Biology

for the Degree of Master of Liberal Arts in Extension Studies

Harvard University

May 2018

Abstract

Patients with T-cell non-Hodgkin lymphoma (T-NHL) face a particularly poor prognosis and are in desperate need of improved targeted therapies and rational combination strategies, especially in the relapsed/refractory setting. Evasion of apoptosis is a hallmark of cancer cells and contributes to drug resistance and tumor progression (Hanahan & Weinberg, 2000). Thus, activation of intrinsic apoptosis is a promising avenue for treatment of a variety of cancers, and drugs targeting specific parts of the pathway are already in clinical use (Ashkenazi et al., 2017). A common mechanism by which lymphomas evade apoptosis is upregulation of anti-apoptotic BCL-2 family members. MCL-1 is the most universally expressed of the BCL-2 family members across a panel of different T-NHL subtypes (Spinner et al., 2016), making it an attractive target in T-NHL. Here we characterize the BCL-2 family members by protein abundance, RNA expression, and copy number variations across a set of 21 T-NHL cell lines and 5 patient-derived xenograft models. To functionally assess the intrinsic apoptosis pathway, we utilized a functional assay called BH3 profiling. BH3 profiling identified MCL-1 dependence across multiple subtypes of T-cell lymphomas. Subsequently we tested the *in vitro* activity of an MCL-1 inhibitor, AZD5991, using a luminescent cell viability assay. As predicted by BH3-profiling, 15 of 21 tested cell lines showed sensitivity to AZD5991. In contrast, there was little correlation between drug sensitivity and either MCL-1 protein abundance or RNA expression. The *in vivo* efficacy of MCL-1 inhibition in PDX models of T-NHL correlated with functional dependence on MCL-1, as measured by BH3

profiling. These data provide support for a biomarker-driven therapeutic approach to select T cell lymphomas that are dependent on MCL-1.

Acknowledgements

This research was made possible by a great many people working together. Many thanks to Sara Morrow, Alexandria Van Scoyk, Dr. Jennifer Crombie, Dr. Samuel Ng, Dr. Noriaki Yoshida, and Dr. Wenchao Wu for technical assistance and advice throughout these experiments. Thank you to Dr. Giorgio Inghirami for his generous donation of WCTL-91953, an anaplastic large cell lymphoma patient-derived xenograft used extensively in this research. Thank you to AstraZeneca for their support and for supplying AZD5991 for these experiments, especially Dr. Alwin Shuller, Dr. Justin Cidado, and Dr. Paul Secrist.

Many thanks and much love to my husband Daniel Poster, for his support and sense of humor.

My unending thanks and appreciation to Dr. Raphael Koch, without whom this research would not have been possible. He is a wonderfully patient and conscientious teacher who cares deeply about the work and the people he works with. He has taught me so much over the past year and I will be forever enriched by my collaboration with him on this project.

Most importantly, I owe a debt of gratitude to Dr. David Weinstock for years of support as a friend and mentor. He is a large part of the reason I am achieving this degree, and he has pushed me to grow technically and intellectually during my time working with him. His generosity is unrivaled. I will be eternally grateful for his friendship and will carry forward everything I have learned from him.

Table of Contents

List of Tables

List of Figures

Chapter I

Introduction

T-cell Non-Hodgkin Lymphoma

T-cell non-Hodgkin lymphomas (T-NHL) are a rare and heterogeneous group of lymphoid malignancies arising from post-thymic or mature T lymphocytes or natural killer (NK) cells. These diseases account for approximately 5-10% of all lymphomas. The World Health Organization currently defines 29 subtypes of T- and NK-cell lymphomas (Swerdlow et al., 2016). Most commonly, T-cell lymphomas are divided into cutaneous T-cell lymphomas (CTCL) and peripheral T-cell lymphomas (PTCL). While CTCLs originate in the skin and generally show an indolent course, PTCLs show an aggressive biology and are associated with very poor prognosis (Foss et al., 2011). The relative rarity of these diseases has hindered progress toward rational treatment strategies, as access to clinical samples and preclinical models is limited, while at the same time the heterogeneity across subtypes precludes a universal standard of care.

T-cells comprise 10-25% of white blood cells and are involved in cell-mediated immunity. T-NHL develops from these post-thymic T lymphocytes. Patients initially present with symptoms such as enlarged lymph nodes, night sweats, bone or chest pains, and fever. Bone marrow or lymph node biopsies are commonly used to diagnose lymphomas while medical imaging is used for disease staging and to monitor progression or regression after therapy. The average age at initial diagnosis is 65-75 years with only 10-30% of patients surviving 5 years post-diagnosis (Zhang et al., 2016).

Patients with these diseases face generally poor outcomes when treated with current regimens, with more primary refractory cases and shorter progression-free survivals as compared to patients with aggressive B-cell lymphomas (Lunning & Horowitz, 2013). Except for young patients with anaplastic large cell lymphomas that harbor rearrangements of the *ALK* gene (ALK+ ALCL), the majority of T-NHL patients relapse rapidly after standard first-line therapy. First-line therapy follows a treatment approach similar to that of diffuse large B-cell lymphoma, specifically CHOP (cyclophosphamide, doxorubicin, vincristine, and prednisone) or a CHOP-like regimen, often followed by consolidation with high-dose chemotherapy and stem cell transplantation (SCT). However, approximately 50% of patients do not achieve a complete remission and most of those who do will relapse after chemotherapy. Treatments for relapsed/refractory T-NHL are particularly problematic and patients with relapsed PTCL have a dismal prognosis with a median overall survival of less than 6 months (Mak et al., 2013).

In Alk+ ALCL the standard CHOP or CHOEP (CHOP plus etoposide) therapeutic regimens often lead to durable remissions and SCT is only advised in high-risk cases (Lunning and Horowitz, 2013). Outcomes from this regimen in other subtypes of T-NHL have not been as favorable and the National Comprehensive Cancer Network still recommends clinical trials as first-line therapy for all of these diseases with the exception of ALK+ ALCL (Zhang et al., 2016). In the relapsed/refractory setting brentuximab vedotin, romidepsin, belinostat, and pralatrexate are approved and have produced some

durable remissions, but more clinical trials are needed in both the up-front and relapsed/refractory settings. Because CHOP remains the most commonly used therapy and can cure a subset of patients, a common strategy is to combine new targeted agents with CHOP, with the hope that this will increase the rate of complete response and possibly cure.

The Intrinsic Apoptosis Pathway

Apoptosis maintains cellular integrity and tissue homeostasis in healthy tissues and is dysregulated in a variety of cancers. The intrinsic apoptotic pathway (Figure 1) is activated in response to cellular stress, such as DNA damage, hypoxia, or metabolic stress; it operates via the release of cytochrome c and second mitochondria-derived activator of caspases (SMAC) from the inner mitochondria. Cancer cells often undergo significant DNA damage and are exposed to nutrient and oxygen-deprived environments due to their increased proliferation rate and metabolic demands, which under normal circumstances would trigger the intrinsic apoptotic pathway. However, evasion of apoptosis is considered a hallmark of cancer as described by Hanahan and Weinberg (2000), emphasizing its importance in neoplastic transformation and disease progression. Besides loss of the apoptosis effectors BAX and BAK or downregulation of pro-apoptotic activators BIM and BID, overexpression of anti-apoptotic BCL-2 family members helps cancer cells avoid death (Figure 2) (Fernández-Marrero et al., 2016).

The pro-survival BCL-2 family members BCL-2, BCL-xL, and MCL-1 contribute to tumor maintenance, progression, and chemoresistance across a range of cancers but

their contributions in distinct subtypes of T-NHL are poorly understood. Immuno-histochemical analyses of T-NHL specimens have revealed a distinct expression pattern of BCL-2 family members, most notably the high expression level of MCL-1 in up to 65% of certain T-NHL entities. High expression of MCL-1 confers poor prognosis in a variety of cancers, including lung, ovarian, and oral cancers, among others (Chowdry et al., 2016; Shigemasa et al, 2002; Palve et al., 2014). Previous studies have highlighted different BCL-2 family members for their functional relevance in specific clinical or preclinical settings. High expression of BCL-2 protein is associated with unfavorable prognosis in T-NHL (Li et al., 2011) and knockdown of even one MCL-1 allele inhibits T-cell lymphoma survival in two transgenic mouse models (Spinner et al., 2016). However, comprehensive functional characterization of the BCL-2 family in T-cell lymphomas is still missing.

Inhibition of BCL-2 Family Members as Treatment in T-cell Lymphoma

BH3-mimetic drugs are a new class of anticancer agents that target anti-apoptotic BCL-2 family members and recently, the BCL-2 inhibitor venetoclax was approved by the Food and Drug Administration for the treatment of patients with chronic lymphocytic leukemia. Venetoclax, and navitoclax (dual BCL-2 and BCL-XL inhibitor) have produced compelling preclinical and clinical data in a variety of hematologic malignancies, such as multiple myeloma, Waldenstrom macroglobulinemia, acute myeloid leukemia, acute lymphoblastic leukemia, and non-Hodgkin lymphoma (Gibson & Davids, 2015).

MCL-1 inhibitors amenable to *in vivo* administration were only recently developed (Kotschy et al., 2016) and are now entering clinical trials. In a research collaboration with AstraZeneca, our lab was provided with a novel MCL-1 inhibitor, called AZD5991. We hypothesize that a significant portion of T-NHL is MCL-1 dependent and could be effectively treated with an MCL-1 inhibitor. To identify a predictive biomarker of response, we comprehensively characterized the expression levels and protein abundance of the BCL2 family, alongside BH3 profiling as a functional approach, and correlated these data with the *in vitro* activity of the MCL-1 inhibitor AZD5991.

Preclinical *In vivo* Models of T-cell Lymphoma

We used a panel of PDX models with varying BCL-2 family dependencies to test the hypothesis that our drug of interest, AZD5991, would promote apoptosis in MCL-1 dependent models and conversely, not promote a response in a model dependent on BCL-xL. We have chosen to use PDX models because traditional cell line xenograft models are often poor predictors of response to drugs in humans and for some subtypes of PTCL, like angioimmunoblastic T-cell lymphomas (AITL), there are no established cell lines available. The reasons for differential response to drugs are not completely understood, but adaptation to *in vitro* growth conditions over many passages may lead to biological changes in cells that make them less representative of heterogeneous human tumors (Hidalgo et al., 2014). PDX models circumvent some of the problems surrounding cell lines due to maintenance *in vivo* rather than in culture; such models may more faithfully

recapitulate histologic and genetic attributes of the donor tumors, and when implanted orthotopically, may be more reflective of human disease. As an example, a study comparing gene expression profiles of a primary small-cell lung cancer tumor and both the PDX and cell line derived from that tumor show irreversible transcriptional changes in the cell line, while the PDX gene expression was similar to the primary tumor (Daniel et al., 2009).

To address the lack of T-NHL preclinical models our team developed a panel of orthotopic PDX models that serially passage by intravenous injection and engraft in the spleen, bone marrow, liver, and/or lymph nodes of injected mice (Townsend et al., 2016; www.proxe.org). These models represent multiple subtypes of T-NHL, including AITL, T-cell prolymphocytic leukemia (T-PLL), CTCL, NK/T-cell lymphoma, and hepatosplenic T-cell lymphoma (HSTCL), and in some cases represent the first ever reported PDX models of these diseases. We additionally acquired subcutaneous PDX models of Alk+ ALCL from a collaborator. The PDX models have undergone whole transcriptome sequencing (RNAseq) and immunoblotting to assess the expression levels and protein abundance of BCL-2 family members and BH3 profiling to determine their individual dependencies on BCL-2 family members. Interestingly, prior data from our lab indicated that protein levels of BCL-2 family members do not necessarily correlate with dependencies (Figure 3).

Research Aims and Hypothesis

There are two goals of this research. First, we aim to characterize preclinical T-NHL models with respect to BCL-2 family members *in vitro* and determine which technical approach is more predictive of sensitivity to a specific MCL-1 inhibitor, AZD5991, and thus may be a useful biomarker for selecting the right drug for a patient. Second, we aim to determine *in vivo* efficacy of AZD5991 in a panel of PDX models alone and in combination with CHOP therapy. Based on previous literature, we hypothesize that BH3 profiling will most accurately predict both *in vitro* and *in vivo* sensitivity to AZD5991 as compared to protein abundance, RNA expression level, and copy number variation. We also hypothesize that the combination of AZD5991 plus CHOP will have superior efficacy to either therapy alone in MCL-1-dependent PDX models, as determined by tumor burden at a pharmacodynamic (PD) time-point and/or increased survival of the combination-treated mice. These studies are intended to inform the clinical use of AZD5991 by supporting its use in combination with CHOP and defining the utility of biomarkers for patient selection.

Chapter II

Materials and Methods

Cell lines

SR786, KIJK, SUPM2, SUDHL1, L82, and DERL2 cells were obtained from DSMZ, Karpas299, Karpas384, MyLa cells from Sigma-Aldrich, HUT78 and MJ from ATCC, DL-40, MTA and KHYG-1 cells from JCRB. FEPD, MAC2A, OCI-Ly13.2 and OCI-Ly12 were kindly provided by Leandro Cerchietti (Weill Cornell Medicine, New York, USA) and NKL cells by Jerome Ritz (Dana-Farber Cancer Institute, Boston, USA). HH cells were provided by Anthony G Letai (Dana-Farber Cancer Institute, Boston, USA) and SMZ1 cells by Hitoshi Ohno (Tenri Medical Institute, Tenri, Japan). Cells were cultured according to the vendor's recommendation. Cell lines were routinely tested for mycoplasma (ATCC® Universal Mycoplasma Detection Kit) and authenticity was validated by short tandem repeat (STR)-profiling.

Western Blots

Sample preparation of whole cell lysates, SDS-PAGE, membrane transfer and blotting were performed as previously (Yoda et al., 2015). Quantification of western blot signals was performed with ImageJ (NIH). Primary antibodies used: mouse mAb α-tubulin (Sigma Aldrich #T9026), mouse mAb BCL-2 (BD Pharmigen #51-6511GR), rabbit mAb BLC-xL (Cell Signaling #2762S), rabbit mAb Bax (Cell Signaling #5023S),

rabbit mAb Bak (Cell Signaling #6947S), rabbit mAb Bim (Cell Signaling #2933S), and rabbit mAb MCL-1 (Santa Cruz Biotechnologies #sc-819).

RNA Sequencing and Analysis

RNA-Seq was performed as described previously (Townsend et al., 2016). Heatmaps were generated with Morpheus (https://software.broadinstitute.org/morpheus).

DNA Sequencing and Copy Number Variant Analysis

Whole exome sequencing and copy number analysis were performed by the Cancer Cell Line Encyclopedia Platform at the Broad Institute as described previously (Barretina et al., 2012).

BH3 Profiling

To understand which anti-apoptotic BCL-2 family member(s) T-cell lymphomas are most dependent on for survival, we subjected a number of T-NHL cell lines, PDX tumors, and patient specimens to an assay called BH3 profiling (Figure 4). BH3 profiling is a technique that allows for functional assessment of how "primed" (close) cells are toward undergoing mitochondrial outer membrane permeability (MOMP). Upon permeabilization of a cell with very low concentrations of digitonin, a library of BH3 peptides that mimic the BH3 domain of specific BCL-2 family members is utilized to

manipulate components of the mitochondrial apoptosis pathway. After incubation with these peptides, the cells undergo fixation and cytochrome c is stained with a fluorescent-labeled antibody. This allows for assessment of cytochrome c release as a marker for MOMP in response to certain BH3 peptides by flow cytometry and identification of mechanisms by which cells evade apoptosis (Ryan et al., 2016; Potter & Letai, 2016). By utilizing BH3 peptides that selectively bind and antagonize anti-apoptotic BCL-2 family members, BH3 profiling allows for the determination of which anti-apoptotic BCL-2 family members cells or tumors are dependent on for survival, which makes it a powerful tool for selecting which specific BH3 mimetic may be appropriate to treat a patient's tumor (Ryan et al., 2016).

For our experiments we used either fresh cells from cell lines or freshly thawed, previously viably frozen PDX cells (for baseline BH3 profiling) and performed BH3 profiling as described previously (Ryan et al., 2016). Peptide concentrations are shown along the X axis in figures. Panels of peptides were used, most importantly including: BIM (exhibits the most broad-ranging BCL-2 protein interactions, engaging all of the antiapoptotic proteins with high affinity and assesses if BAX and BAK are present and functional), Bad (interacts with BCL-2, BCL-xL and BCL-w), HRK (interacts with BCL-xL), and MS1 (interacts with MCL-1). A titration of BIM peptide provides data on the overall priming of cells since it inhibits all major anti-apoptotic proteins of interest. Dimethyl sulfoxide (DMSO) is used as a negative control, as it should not induce apoptosis. Alamethicin is a channel-forming peptide antibiotic that forms transmembrane pores in the mitochondria, thus acting as a positive control.

CellTiter-Glo® Analysis

Viable cells were plated in white opaque 384-well plates using an EL406 Combination Washer Dispenser (BioTek) at a density of 1.5x10^5 cells per ml. AZD5991 was added using a JANUS Automated Workstation (PerkinElmer). For growth curve analysis, cells were incubated for 72h before CellTiter-Glo Luminescent Cell Viability reagent (Promega) was added to each well according to the manufacturers protocol and read by the 2104 EnVision Multilabel Reader (PerkinElmer) as described previously (Weigert et al., 2012). Each data point represents quadruplicates and experiments were repeated at least twice.

Apoptosis Analysis by Annexin V/7-AAD

Apoptosis assay was performed per manufacturer's FITC Annexin V Apoptosis Detection Kit with 7-AAD (BioLegend) experimental protocol.

Caspase Activation Assay

Caspase activation assay was performed per manufacturer's Caspase-Glo® 3/7 Assay (Promega) experimental protocol.

In vivo Modeling of T-cell Lymphomas

All *in vivo* experiments were conducted under Dana-Farber Cancer Institute Animal Care and Use Committee protocol #13-034 and Public Health Service animal assurance #A3023-01. Animal work was performed in Nod.CgPrkdc^{scid}IL2rg^{tm1Wjl}/SzJ (NSG) mice purchased from Jackson Laboratories. A full description of each PDX model is available online at the Public Repository of Xenografts (www.PRoXe.org), including clinical history, genomic data, etc. Viably frozen PDX cells were thawed and washed in 1x PBS before tail-vein injection at 0.7–1.0 x 10^6 cells per mouse. For subcutaneous models, tumor fragments were implanted in the right flank under isoflurane anesthesia. Tumor burden was monitored periodically based on engraftment kinetics of each model by flow cytometry of peripheral blood or tumor size by digital caliper measurement for subcutaneous models. Tumor size was measured in two perpendicular dimensions, and volume was calculated as [(Longest dimension x perpendicular dimension^2)/2].

When mice were sufficiently engrafted they were randomized into treatment arms by peripheral blood disease or tumor volume so that each arm contained mice with approximately the same mean tumor burden. Drugs were dosed as described in the section: *In vivo* Administration of Therapeutic Regimens and protocols for flow cytometry are described in the section: Fluorescence Activated Cell Sorting of Mouse Blood. Mice were monitored daily for clinical signs of disease and humanely euthanized when they reached a clinical endpoint or a subcutaneous tumor reached 2cm in the longest dimension.

Flow Cytometry of Mouse Blood

Fifty microliters of mouse blood per mouse was processed with 2ml Red Blood Cell Lysis Buffer (Qiagen 158904) before staining with antibodies against human CD45 (Pacific Blue V450-conjugated, BD Bioscience 560367) and human CD2 (APC-conjugated, BioLegend 300213) or human CD56 (APC-conjugated, BD Bioscience 555518) in 1x PBS with 1mM EDTA plus 1% fetal bovine serum. Live cells were gated in the forward scatter versus side scatter plot and subsequent analysis was done on this population, with 5,000 to 10,000 total events captured per sample. SMZ-1 unstained cells were compared to single stained SMZ-1 cells to set voltages for each antibody. All stained mouse blood samples were compared to an unstained mouse blood sample to control for possible autofluorescence. Flow cytometry data was analyzed with FlowJo software. Only CD45 and CD2 double positive cells were used to calculate percent peripheral blood involvement.

In vivo Administration of Therapeutic Regimens

Drug doses, vehicle, and schedule are shown in Table 1. All drugs were administered in a volume of 10ml/kg based on each animal's body weight, which was measured at least twice weekly. Dosing was temporarily held for any mouse that lost 15% body weight compared to day 1 of treatment, and if the mouse regained weight it was re-enrolled on therapy. Mice that lost 15% body weight on treatment were given daily subcutaneous fluids (5% dextrose in water; 500ul volume) and supplemental high

calorie diet (Nutrical). Drugs were administered using a 1 ml syringe with 27-gauge needle. Mice in the vehicle arm on trials comparing only AZD5991 received Vehicle 1. Mice in the vehicle arm on trials comparing AZD5991 plus CHOP combination therapy received Vehicle 1 and Vehicle 2.

Biostatistics

Survival outcomes were calculated using the Log-Rank test. P-values for comparisons between grouped data (such as organ size and peripheral blood disease) were calculated by unpaired two-sided t-tests. For correlations, we calculated the nonparametric Spearman correlation coefficient (r). The above tests were performed using GraphPad Prism software. Microsoft Excel was used to graph mean tumor volume and peripheral blood disease longitudinally; error bars represent standard error of the mean (SEM; Figures 15, 21 and 28).

Chapter III

Results

In vitro

We first characterized the mitochondrial apoptosis pathway across 21 T and NK cell lines, focusing on effectors BAX and BAK, the activator BIM, and anti-apoptotic proteins BCL-2, BCL-xL, and MCL-1. Western blot analysis identified a pattern of high MCL-1 protein abundance in Alk+ and Alk- ALCL lines, whereas CTCL lines generally had higher levels of BCL-xL (Figure 5). Cells lines next underwent RNA sequencing to assess expression levels of the same pathway components. RNA expression levels (as Reads Per Kilobase of transcript per Million mapped reads, or RPKM) were plotted against quantified protein abundance and are shown in a correlation matrix (Figure 6). There was a correlation between expression level and protein abundance, as shown by the linearity of the correlation ($r=-0.6679$) and p-value (<0.0001). DNA from these cell lines underwent exome sequencing, which allows for assessment of copy number variations. The most significant amplification of MCL-1 was found in Karpas299, with lesser gains in SMZ1 and Karpas384 (Figure 7). The amplifications in SMZ1 and Karpas299 are in alignment with the high levels of MCL-1 protein and RNA transcript seen in those cell lines. Conversely, MCL-1 expression and protein level were low in Karpas384, suggesting that copy number variations may not predict the functional relevance of this protein.

There are multiple ways by which cells can dysregulate the intrinsic pathway of apoptosis. First, loss of the effectors BAX/BAK will likely lead to no depolarization even when pro-apoptotic activators (BIM/BID) and sensitizers (Bad, HRK, MS1) are present. Second, the loss of activators BIM/BID would prevent apoptosis in the presence of sensitizers, but depolarization would occur if BIM/BID were added to the system. Lastly, overexpression of anti-apoptotic BCL-2 family members (such as BCL-2, BCL-xL, and MCL-1) can be overcome by introduction of both sensitizers and activators. To assess these possibilities, BH3 profiling was conducted on all cell lines (Figure 8).

For nearly all lines, adding the pro-apoptotic activator BIM (in various concentrations) led to induction of cytochrome c release. A notable exception is Hut78 where even high doses of BIM led to only moderate release of cytochrome c. This is in line with the loss of BAX and very low BAK expression in this cell line (Figure 5). Specific pro-apoptotic sensitizers (such as Bad, Hrk, and MS1) differentially induced cytochrome c release across cell lines, suggesting that specific anti-apoptotic BCL-2 family members (BCL-2, BCL-xL, MCL-1) blocked apoptosis in multiple T-NHL subtypes. However, which BCL-2 family member blocks apoptosis in each line is heterogeneous. BCL-xL, possibly in cooperation with BCL-2, was the primary dependence in CTCL lines. The MCL-1-binding peptide MS1 induced cytochrome c release across multiple subtypes, including 9 out of 10 ALCL lines. Importantly, MTA and HH cell lines showed strong MCL-1 dependence by BH3 profiling but low RNA expression and protein abundance, and no copy number gains. We hypothesized that dependence as determined by BH3 profiling would be a superior predictor of sensitivity to MCL-1 inhibition as compared to the other types of characterization discussed above.

To determine *in vitro* sensitivity to MCL-1 inhibition, we subjected cell lines to treatment with the specific MCL-1 inhibitor AZD5991 (AstraZeneca). Half maximal inhibitory concentration (IC50) was determined using the CellTiter-Glo® chemiluminescence assay. Fifteen of 21 cell lines had submicromolar sensitivity to AZD5991 (Figure 9). We next created correlation matrices comparing IC50 values of each cell line compared to its MCL-1 protein abundance, RNA expression, or cytochrome c release after incubation with MS1 peptide (Figure 10). AZD5991 IC50 showed no correlation with MCL-1 protein abundance ($r=-0.018$), while there was weak correlation between IC50 and RNA expression level ($r=-0.4688$, $p=0.0320$). There was a strong correlation between IC50 and cytochrome c release induced by the MS1 peptide as measured by BH3 profiling ($r=-0.7208$, $p=0.0002$).

Finally, we incubated a subset of cell lines with AZD5991 at 250nM and 1uM to assess induction of apoptosis at 4 hours and 6 hours (Figure 11, representative cell lines shown). Early apoptosis is indicated in this assay by the Annexin V positivity while late apoptosis is indicated by positivity for both Annexin V and 7-AAD. BH3 profiling predicted that SMZ1 would be highly sensitive to MCL-1 inhibition, which was confirmed by complete induction of apoptosis at 4 hours in even the low dose of AZD5991. Karpas299 was predicted to be moderately sensitive to MCL-1 inhibition, which was confirmed by the dose-dependent sensitivity to AZD5991. Hut78 showed no induction of apoptosis by BH3 profiling and, as expected, was completely resistant to MCL-1 inhibition in this assay.

In vivo

Our *in vitro* assays demonstrated a common MCL-1 dependence across ALCL cell lines (9 out of 10), which was also true of our PDX models of ALCL. WCTL-91953 is an Alk+ ALCL whose baseline BH3 profile indicated MCL-1 dependence (Figure 12). As an initial *in vivo* experiment, we implanted tumor fragments of this model subcutaneously and initiated therapy when tumors reached an average of 550 mm^3. Mice were randomized to receive Vehicle 1 or AZD5991 single dose and three mice per arm were euthanized for pharmacodynamic (PD) analysis 24 hours after the first dose. We calculated the percentage of tumor weight compared to each mouse's body weight (Figure 13). WCTL-91953 mice treated with AZD5991 had smaller tumors compared to body weight 24 hours after dosing but due to variation among the vehicle-treated mice this difference was not significant ($p=0.127$). Remaining mice were treated weekly with AZD5991 or vehicle and euthanized when their tumor reached 2 cm in the longest dimension; mice treated with AZD5991 had significantly prolonged survival compared to vehicle-treated mice (Table 2). Measurement of tumor volumes illustrated that each weekly treatment with AZD5991 significantly reduced tumor size but tumors rapidly regrew prior to the next dose (Figure 14). These tumor volume data led us to increase the frequency of AZD5991 dosing to days 1 and 2 of each week (based on data from AstraZeneca); this dosing strategy was utilized in the subsequent experiments below.

Concurrently with the above experiment we treated another PDX, DFTL-78024, with single dose AZD5991 once weekly until sacrifice. DFTL-78024 is a model of AITL and has mixed dependency on MCL-1 and BCL-xL as determined by cytochrome c

release after incubation with both MS1 and Bad peptides. As expected, treatment of DFTL-78024 cells *ex vivo* with AZ-5991 induced apoptosis (measured by caspase 3/7 activation) while treatment with the BCL2 inhibitor ABT-199 did not (Figure 17). This model engrafts in the spleen, bone marrow, cervical lymph nodes, and peripheral blood. When the average peripheral blood engraftment was 6%, mice were randomized to receive AZD5991 single dose or Vehicle 1. Three mice per arm were euthanized 24 hours after the first dose for PD analysis. Peripheral blood disease at this time-point was not significantly reduced in mice treated with AZD5991 compared to vehicle (Figure 18). Blood cells were also incubated with BIM to assess overall apoptotic priming of tumor cells after one dose of AZD5991, with residual tumor cells in the drug-treated mice being only slightly more primed ($p=0.1179$, Figure 19). This did not translate into a survival advantage for drug-treated mice, and a subsequent study using AZD5991 double dose also did not confer a survival advantage in this model (Table 2). Thus, despite the evidence of MCL-1 dependence in this model by BH3 profiling, there was minimal *in vivo* benefit from AD5991 treatment.

Next, we combined the double dose regimen with CHOP in a subset of models (dosing regimen described in Table 1). Tumor volume data demonstrated that increasing AZD5991 to twice weekly did not lead to more durable tumor remissions in mice engrafted with WTCL-91953 (Figure 15). However, addition of CHOP therapy to AZD5991 significantly prolonged tumor regression and extended survival compared to either CHOP alone or AZD5991 alone (Figures 15 and 16, Table 2). Three combination mice were sacrificed when moribund but had no visible or palpable tumors at the time of euthanasia. Necropsy of these three mice revealed significantly shrunken livers but no

obvious disease; fixed liver samples have been sent for hematoxylin & eosin staining and immunohistochemistry for disease markers to confirm the liver phenotype is not due to disease burden, but rather a result of delayed toxicity. These data are pending.

We next treated additional models with double dose AZD5991 weekly plus CHOP as above. CBTL-81777 is a model of hepatosplenic T-cell lymphoma that engrafts in the liver, spleen, bone marrow, and peripheral blood. This model has mixed dependency, with the most significant cytochrome c release triggered by incubation with MS1 peptide, indicating a primary MCL-1 dependence (Figure 20). When peripheral blood involvement reached a mean of 0.7%, mice were randomized to Vehicle 1+2, AZD5991 double dose, CHOP, or combination AZD5991 plus CHOP. Mice were bled 7 days after initial dose to assess disease burden (Figure 21). CHOP alone had no effect on blood disease compared to vehicle treatment. Mice treated with AZD5991 had stable disease whereas mice receiving the combination had disease regression. This translated to a significant survival advantage for combination mice compared to vehicle ($p=0.0023$), CHOP ($p=0.0004$), and AZD5991 ($p=0.0048$) (Figure 22, Table 2).

DFTL-22685 is a model of CTCL that engrafts in the spleen, bone marrow, and peripheral blood. This model is primarily MCL-1 dependent, with little cytochrome c release triggered by incubation with Bad or HRK peptides (Figure 23). Due to this model's aggressive course of disease, treatment was initiated at the first sign of peripheral blood disease (~0.02%), at which time mice were randomized to Vehicle 1+2, AZD5991 double dose, CHOP, or combination AZD5991 plus CHOP. Mice treated with combination therapy experienced significant toxicity leading to early euthanasia. Comprehensive tissue analysis is required to determine the exact cause of the toxicity,

which manifested as weight loss >15%, paleness, and severe lethargy. Though we were unable to collect survival data for the combination arm, comparison can be made between vehicle mice sacrificed on day 16 (presumably due to progressive disease) and combination mice sacrificed the same day (presumably due to toxicity). Combination mice had significantly lower disease burden in both spleen ($p=0.0005$) and bone marrow ($p=0.0406$) on day 16 compared to vehicle mice sacrificed on the same day, indicating that combination therapy was highly effective against CTCL cells (Figures 24 and 25). Mice treated with AZD5991 ($p=0.0009$) or CHOP ($p=0.0088$) had significantly prolonged survival compared to vehicle mice (Figure 26, Table 2).

Lastly, DFTL-28776 is a model of T-cell prolymphocytic leukemia that engrafts in the spleen, bone marrow, and peripheral blood. This model is primarily BCL-xL dependent with some BCL-2 dependency (Figure 27), and is predicted to be insensitive to MCL-1 inhibition. Mice were treated with Vehicle 1, AZD5991 single dose, or AZD5991 double dose weekly until sacrifice. On day 7 mice were bled to determine peripheral blood disease burden; there was no significant difference between groups (p-values: vehicle vs. single dose = 0.10, vehicle vs. double dose = 0.34, single dose vs. double dose AZD5991 = 0.55, Figure 28). This was confirmed by survival data showing no difference between vehicle mice and mice treated with AZD5991 single dose or double dose (Figure 29, Table 2).

Chapter IV

Discussion

Significance of Results

Patients with T-cell non-Hodgkin lymphoma (T-NHL) face a particularly poor prognosis and are in desperate need of improved targeted therapies and rational combination strategies, especially in the relapsed/refractory setting. Evasion of apoptosis is a hallmark of cancer cells and contributes to drug resistance and tumor progression (Hanahan & Weinberg, 2000). Thus, activation of intrinsic apoptosis is a promising avenue for treatment of a variety of cancers, and drugs targeting specific parts of the pathway are already in clinical use (Ashkenazi et al., 2017). A common mechanism by which lymphomas evade apoptosis is upregulation of anti-apoptotic BCL-2 family members. MCL-1 is the most universally expressed of the BCL-2 family members across a panel of different T-NHL subtypes (Spinner et al., 2016), making it an attractive target in T-NHL.

Our *in vitro* data characterize the BCL-2 family members across a panel of T-NHL cell lines. Western blot data in our cell lines confirm prior patient sample data describing MCL-1 as commonly expressed in T-NHL, and RNA expression is well correlated to protein abundance of BCL-2, BCL-xL, and MCL-1. However, MCL-1 inhibitors amenable to *in vivo* administration were only recently developed (Kotschy et al., 2016), so there is little data indicating whether protein abundance, RNA expression, or DNA sequencing data are sufficient biomarkers when determining which patients are

most likely to respond to MCL-1 inhibition. Our data indicate that, at least *in vitro,* these biomarkers are insufficient for predicting response. Correlation matrices comparing IC50 values of each cell line treated with the MCL-1 inhibitor AZD5991 compared with its MCL-1 protein abundance or RNA expression showed minimal correlation at best (Figure 10). Previous literature suggests that BH3 profiling may be a superior predictor of sensitivity to BCL-2 family member inhibition (Chonghaile et al., 2014; Montero et al., 2014; Ryan et al., 2016).

BH3 profiling is a technique that allows for functional assessment of how "primed" (close) cells are toward undergoing mitochondrial outer membrane permeability (MOMP). BH3 profiling data in our cell lines identified MCL-1 dependence in a variety of T-NHL subtypes, such as Alk+ and Alk- ALCL, PTCL-NOS, NK/T-cell lymphoma, and CTCL (Figure 8). We also created baseline (untreated) BH3 profiles for a panel of T-NHL PDX models to aid in selecting models for *in vivo* efficacy studies. We chose models with strong MCL-1 dependency (WCTL-91953), mixed dependencies with primary MCL-1 dependence (CBTL-81777, DFTL-22685, DFTL-78024), and a model with primary BCL-xL dependence as a negative control (DFTL-28776). BH3 profiling may be a superior predictor of response but it also identifies mixed susceptibility in models that don't always predict response well. More research is needed to understand if secondary dependencies are upregulated in response to inhibition of the primary pro-survival protein, and what other factors may contribute to limited efficacy in models predicted to be sensitive to AZD5991.

Initial *in vivo* experiments using single dose AZD5991 were conducted in WCTL-91953 and DFTL-78024. Long term monitoring of WCTL-91953 tumor size indicated

that AZD5991 caused tumor regression in all drug-treated mice but tumors regrew rapidly each week; these tumors remained sensitive to each additional dose of AZD5991 (Figure 14). This led us to conduct a second trial using a double dose of AZD5991 alone or in combination with standard of care therapy CHOP. While the double dose of drug did not produce more durable remissions, the addition of CHOP was superior both in maintaining remissions and in overall survival (Figures 15 and 16). The weekly regrowth of tumors in even the double dose study suggests that daily dosing may be more efficacious but this regimen is not well tolerated. The limitation in dosing frequency likely contributes to the limited efficacy seen in some models. Optimized inhibitors amenable to more frequent *in vivo* administration or with more favorable pharmacokinetic properties may lead to superior responses.

DFTL-78024 mice treated with AZD5991 had a decrease in peripheral blood disease at the PD time-point, though this result was not significant due to the heterogeneity of engraftment (Figure 18). These same tumor cells were not significantly more primed toward apoptosis after one dose of AD5991 *in vivo* and there was no survival advantage in drug-treated mice (Figure 19, Table 2). It is possible that the inherent heterogeneity of DFTL-78024 precludes it from being a useful model to study MCL-1 inhibition *in vivo.* Further research may explain why inhibition of MCL-1 was only minimally active in this model, and experiments pursuing the combination with CHOP could be useful in bolstering the activity of AZD5991.

CBTL-81777 mice treated with AZD5991 had stable peripheral blood disease 7 days after the first drug dose, compared to vehicle and CHOP-treated mice that all had a significant increase in disease. Mice treated with a combination of AZD5991 and CHOP

saw disease regression at this time-point (Figure 21). These early differences in disease burden translated to a survival advantage in the combination arm versus vehicle, AZD5991, and CHOP (Figure 22). While CHOP therapy had no effect on disease burden or survival, the addition of CHOP to AZD5991 led to significant survival advantage; this suggests that the combination may be efficacious even in patients refractory to CHOP therapy, and it could be useful to pursue clinically in both CHOP-sensitive and insensitive patient populations.

DFTL-22685 saw a survival advantage in both the AZD5991 and CHOP arms compared to vehicle, but due to toxicity the combination arm was euthanized early (Figure 26). However, comparing disease burden in the spleen and bone marrow at day 16 demonstrated that combination mice had minimal spleen disease and significantly lower bone marrow disease than vehicle-treated mice (Figure 24 and Figure 25). It is unclear why this model experienced such severe toxicity compared to other models. Previous work has shown that doxorubicin dosed intraperitoneally in immunodeficient mice has toxic effects, including liver damage (Wunderlich et al., 2013). This may explain the delayed toxicity seen in combination-treated WCTL-91953 mice. This toxic effect may have been more damaging in a model like DFTL-22685, which presents with highly aggressive bone marrow disease. Our experience indicates that the physiologic stress associated with such PDX models can cause the animals to become more sensitive to additional stressors, making them less able to tolerate an aggressive drug regimen. We have some evidence suggesting that intravenous dosing of doxorubicin is better tolerated and should be used in future experiments. For the purposes of these experiments we kept

the intraperitoneal dosing consistent in all models to limit the number of variables between experiments.

Lastly, we treated DFTL-28776 to demonstrate that a model lacking MCL-1 dependence by BH3 profiling would be insensitive to AZD5991. This model was treated with both single and double dose schedules of AZD5991 compared to vehicle, and the drug did not produce any survival advantage in treated mice (Figure 29). These *in vitro* and *in vivo* data support MCL-1 as an attractive target in T-NHL, especially in combination with cytotoxic chemotherapy.

Study Limitations

This research is limited by the available T-NHL models, especially considering that cell lines do not exist for some subtypes of T-NHL, such as AITL. Of our 21 cell lines, 10 represented either Alk+ or Alk- ALCL, while some other subtypes were represented by only 1 or 2 cell lines. Generalizing BCL-2 family member dependencies by subtype other than ALCL is not possible, though patterns emerged among CTCLs and PTCLs. Additionally, there is a dearth of biologically representative *in vivo* models of T-NHL. To address this, our team developed a panel of orthotopic PDX models that represent multiple subtypes of T-NHL, and in some cases, represent the first ever reported PDX models of these diseases. We additionally acquired subcutaneous PDX models of Alk+ ALCL from a collaborator. This group of PDXs allowed for *in vivo* evaluation of AZD5991, but since the pool of PDXs is relatively small, we were restricted to using MCL-1 dependent models regardless of tractability. For example,

DFTL-78024 has relatively heterogeneous engraftment, which can cause difficulty in interpreting data, but we felt compelled to use this model as it was our only MCL-1 dependent model of AITL with intact BAX and BAK. The toxicity seen in DFTL-22685 combination mice, but not seen in other models, illustrates the complexity of using orthotopic PDX models. Since *in vivo* trials can take months to run from initial injection of tumor cells to survival endpoints, we did not have time to fully address a dose de-escalation to attain optimal effect in this model.

Appendix

Table 1. *In vivo* administration of therapeutic regimens.

Drug	Vehicle	Route	Dose	Schedule
AZD5991	30% hydroxypropyl β-cyclodextran titrated to pH 9.0 with Megalumine	Intravenous	100mg/kg	Day 1 (for single dose) or days 1-2 (for double dose), weekly
Cyclophosphamide	Phosphate-buffered saline	Intraperitoneal	30mg/kg	Single dose, day 1
Doxorubicin	Normal saline	Intraperitoneal	2.48mg/kg	Single dose, day 1
Vincristine	Normal saline	Intravenous	0.38mg/kg	Single dose, day 1
Prednisone	Phosphate-buffered saline	Intraperitoneal	2mg/kg	Days 1-5
Vehicle 1	30% hydroxypropyl β-cyclodextran	Intravenous	10ml/kg	Same schedule as AZD5991
Vehicle 2	Phosphate-buffered saline	Intraperitoneal	10ml/kg	Same schedule as Prednisone

Table 2. Survival outcomes summarized by PDX model. P-values calculated by Log-Rank test using GraphPad Prism. Single dose AZD5991 indicates weekly on day 1. Double dose indicates days 1 and 2 each week.

Model	Disease	Predicted BCL-2 family member dependence	AZD5991 dosing regimen	Benefit from AZD5991 alone	Benefit from CHOP	Benefit from combination (double dose AZD5991) therapy
WCTL-91953	Alk+ ALCL	MCL-1	Single dose | double dose	Single vs. vehicle p=0.0014 | Double vs. vehicle p=0.0071	vs. vehicle p=0.0458	vs. vehicle p=0.0007 | vs. AZD5991 p=0.0015 | vs. CHOP p=0.0005
DFTL-78024	AITL	Mixed MCL-1 and BCL-xL	Single dose | Double dose	vs. vehicle p=0.7818 | vs. vehicle p=0.2153	N/A	N/A
DFTL-22685	CTCL	Mixed MCL-1 and BCL-xL	Double dose	vs. vehicle p=0.0009	vs. vehicle p=0.0088 | vs. AZD5991 p=0.8695	N/A

CBTL-81777	HSTCL	Mixed MCL-1, BCL-2 and BCL-xL	Double dose	vs. vehicle p=0.1490	vs. vehicle p=0.3835 | vs. AZD5991 p=0.005	vs. vehicle p= 0.0023 | vs. CHOP p=0.0004 | vs. AZD5991 0.0048
DFTL-28776	T-PLL	BCL-2 and BCL-xL	Single dose | double dose	Single vs. vehicle p=0.2863 | Double vs. vehicle p=0.2869	N/A	N/A

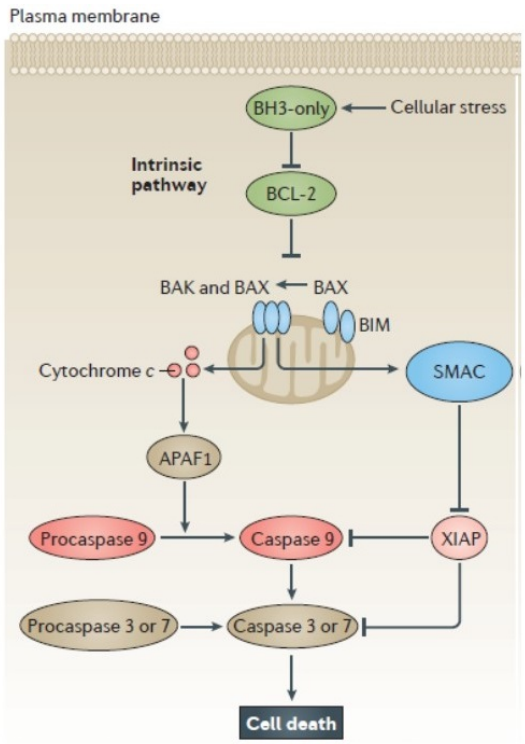

Figure 1. Schematic describing the intrinsic apoptosis pathway (Ashkenazi et al., 2017).

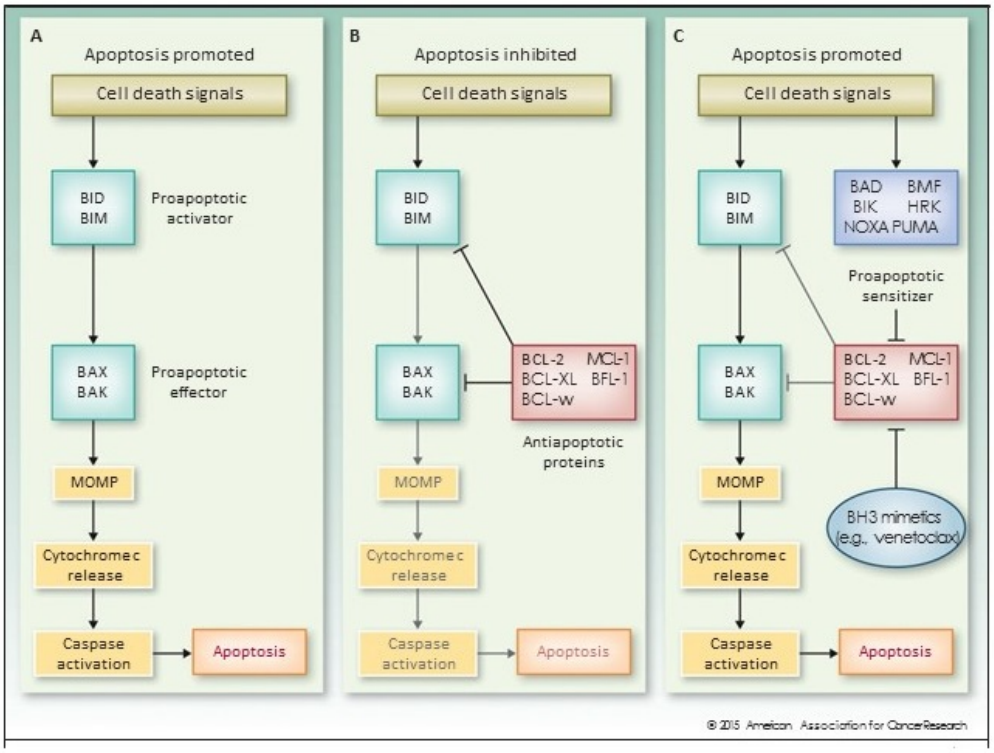

Figure 2. Overview of pro- and anti-apoptotic molecules (Gibson & Davids, 2015).

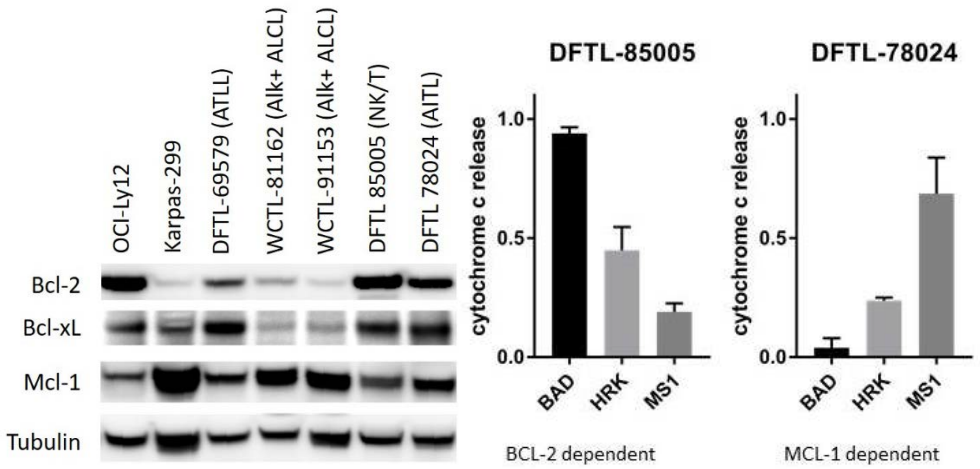

Figure 3. Predictive power of protein abundance versus BH3 profiling to determine BCL-2 family member dependence (*Left)* Western blot for BCL-2 family protein levels in cell lines and PDX-models of T-cell lymphomas. Note that both PDX models DFTL-85005 and DFTL-78024 express BCL-2, BCL-xL and MCL-1 at comparable levels. (*Right)* BH3 profiling shows that DFTL-85005 is primarily BCL-2 dependent with some BCL-xL dependency, while DFTL-78024 is dependent primarily on MCL-1. BAD: peptide against BCL-2 and BCL-xL; HRK: peptide against BCL-xL only; MS1: peptide against MCL-1 only. (unpublished data)

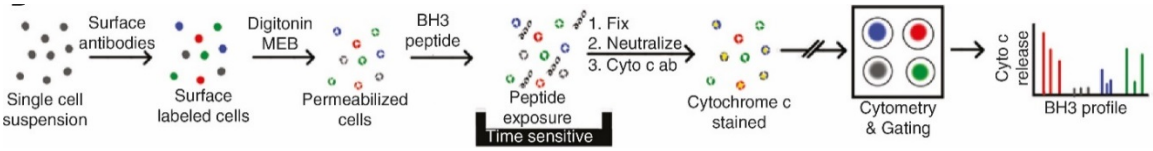

Figure 4. Schematic of BH3 profiling (Ryan et al., 2016).

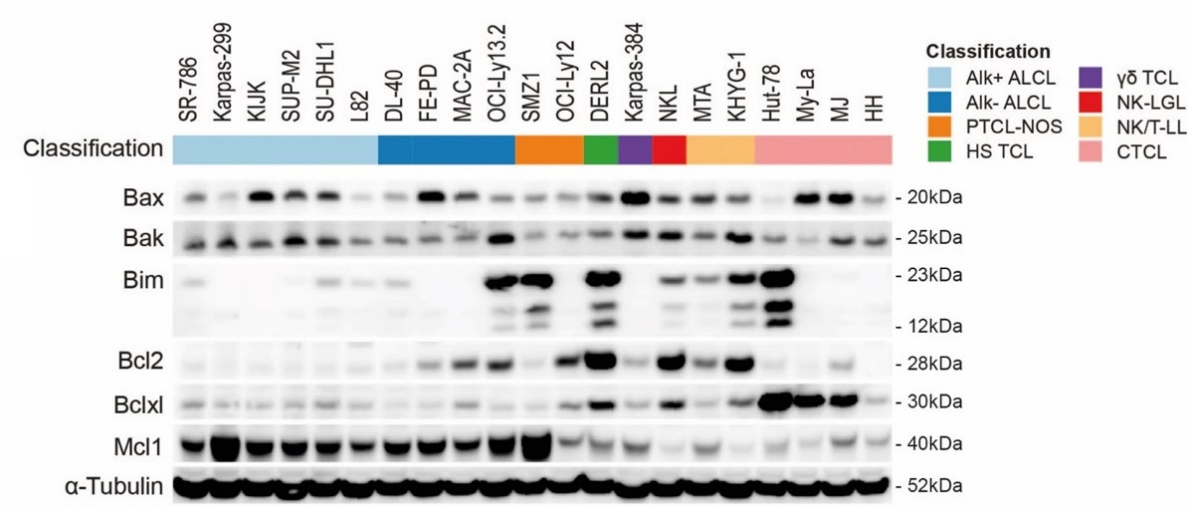

Figure 5. Protein abundance of BCL-2 family members across a panel of 21 T-NHL cell lines.

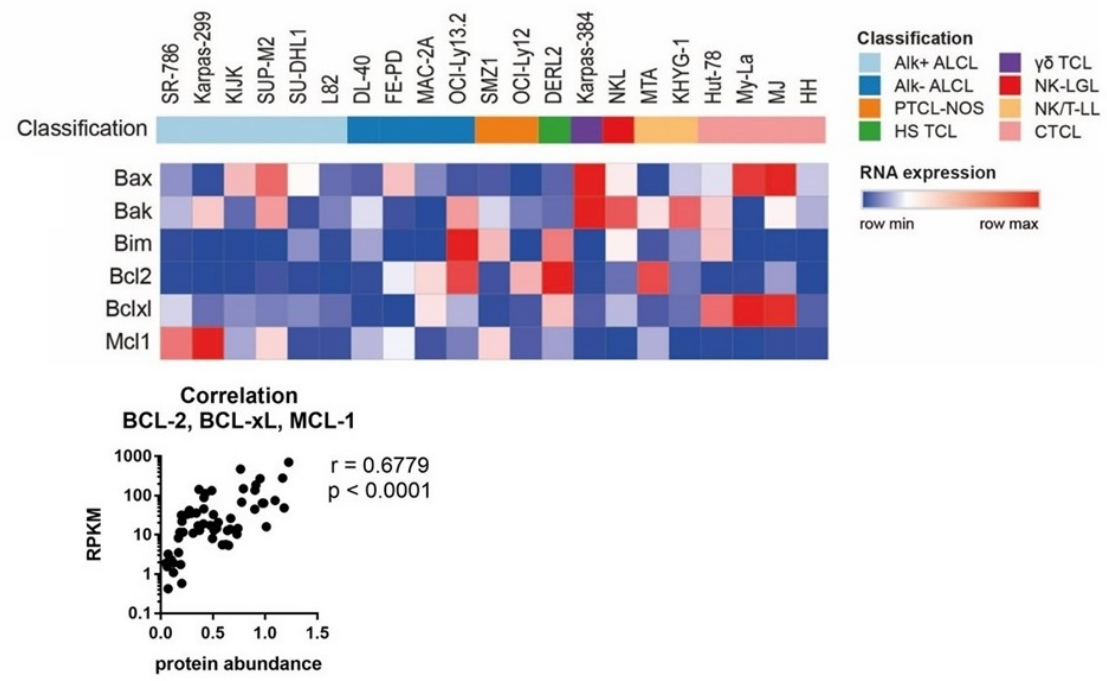

Figure 6. RNA expression levels of BCL-2 family members across a panel of T-NHL cell lines and correlation matrix comparing protein abundance and RNA expression.

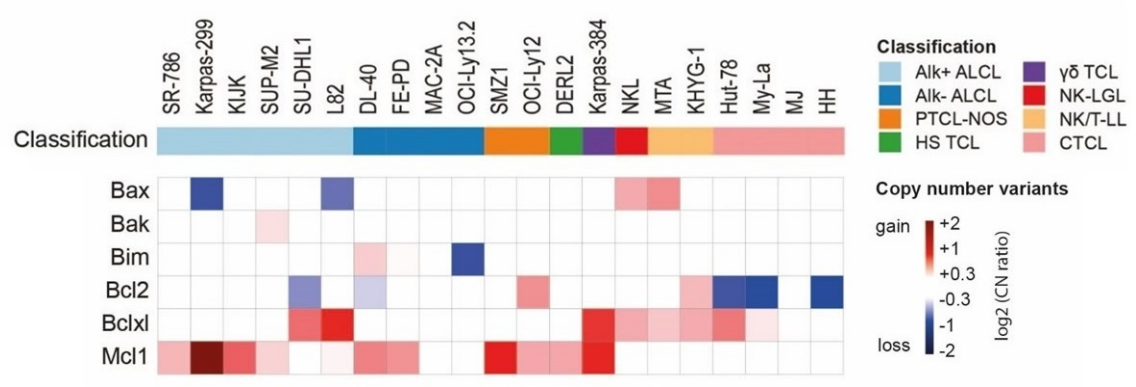

Figure 7. Copy number variations of BCL-2 family members across a panel of 21 T-NHL cell lines.

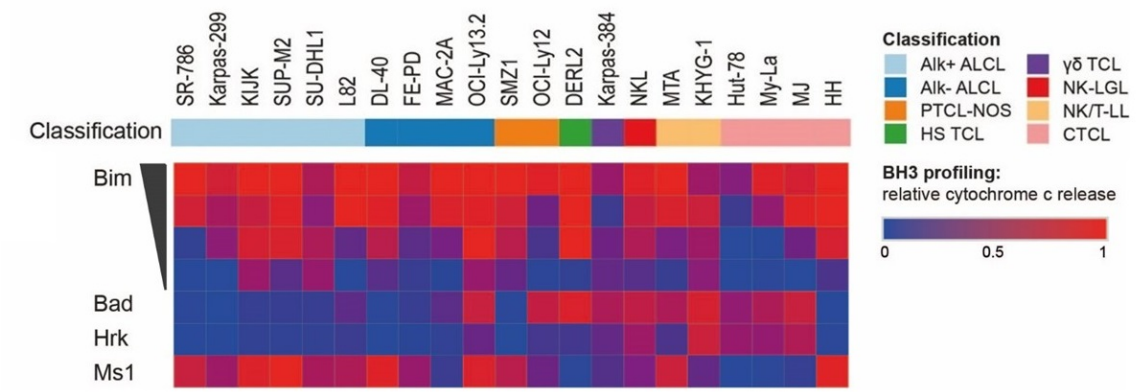

Figure 8. BH3 profiling across 21 T-NHL cell lines indicates dependencies on various BCL-2 family members.

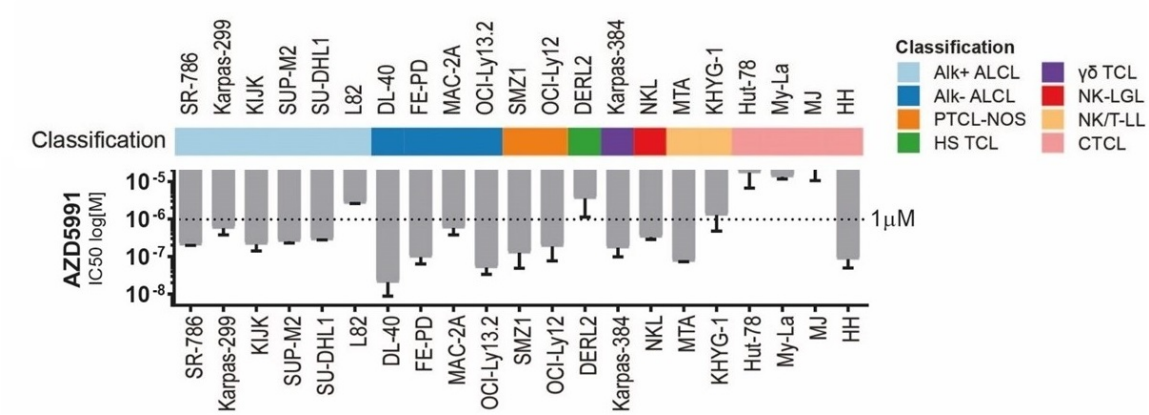

Figure 9. *In vitro* treatment with AZD5991 identifies submicromolar sensitivity (IC50) in 15 of 21 T-NHL cell lines as determined by CellTitre-Glo® assay.

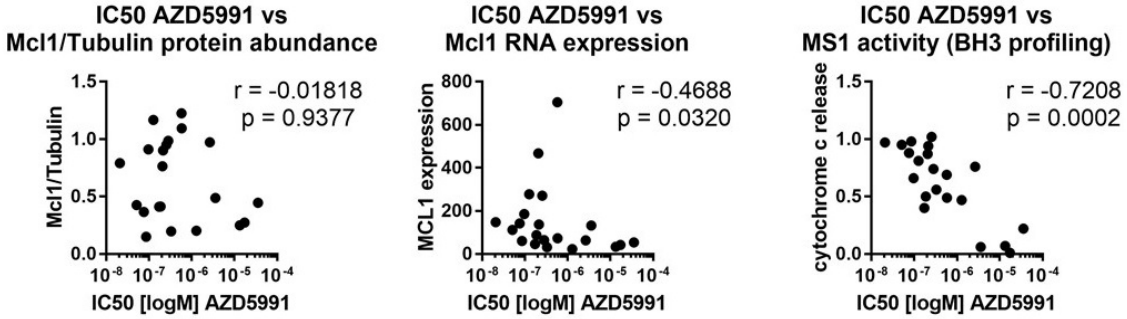

Figure 10. Correlation matrices comparing IC50 values to MCL-1 protein abundance, RNA expression, or cytochrome c release after incubation with MS1 peptide (BH3 profiling). Functional dependence by BH3 profiling most accurately predicts sensitivity to AZD5991 across a panel of 21 T-NHL cell lines.

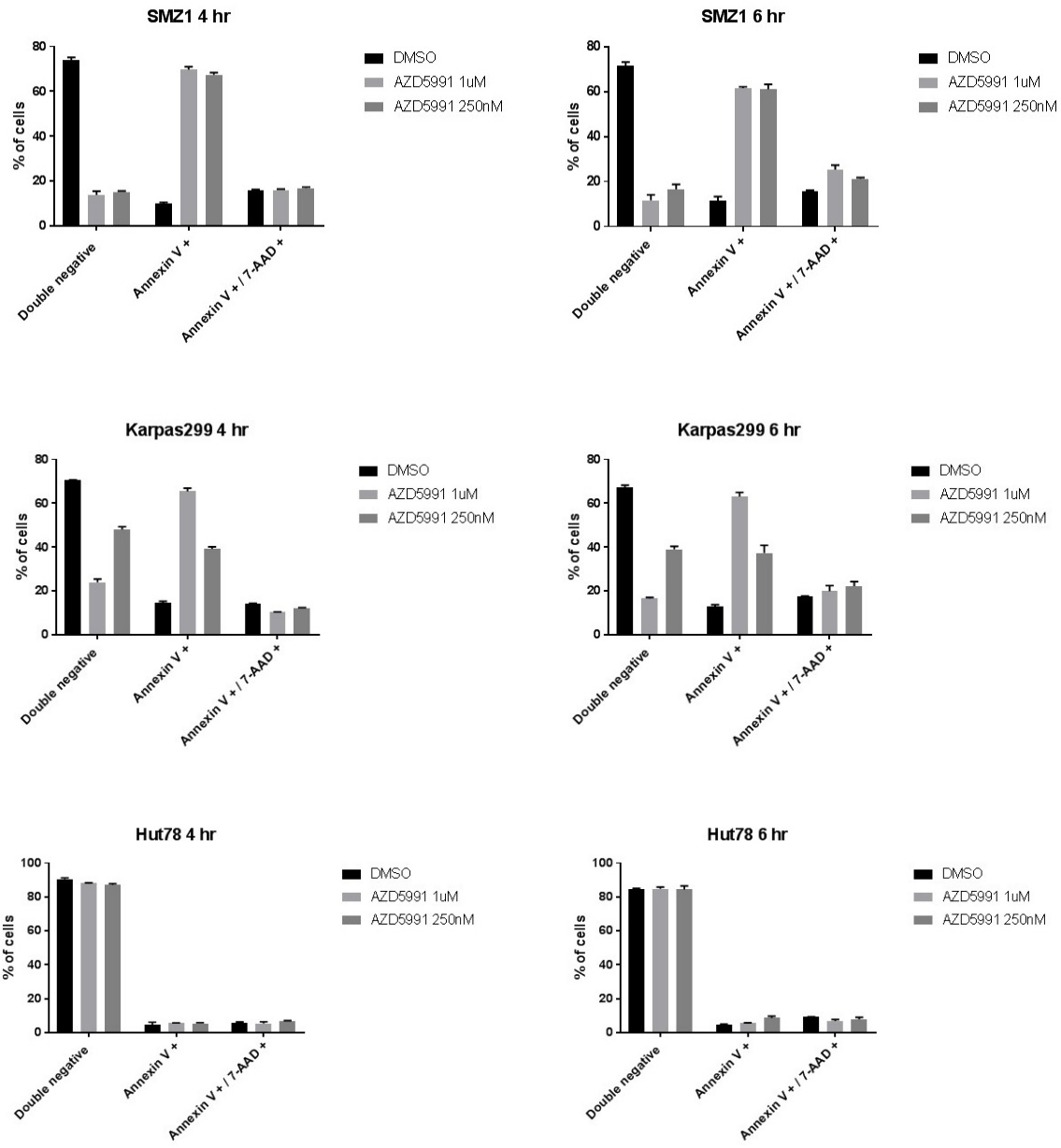

Figure 11. Induction of apoptosis in predicted sensitive T-NHL cell lines as determined by Annexin V/7-AAD FACS analysis. (*Top)* BH3 profiling predicts SMZ1 is highly sensitive to MCL-1 inhibition, which is confirmed by almost complete induction of apoptosis at 4 hours in even the low (250nM) dose of AZD5991. (*Middle)* Karpas299 is predicted to be moderately sensitive to MCL-1 inhibition, which is confirmed by the dose-dependent sensitivity to AZD5991. (*Bottom)* Hut78 shows no induction of apoptosis upon incubation with MS1 peptide by BH3 profiling, and is confirmed to be completely resistant to MCL-1 inhibition in this assay.

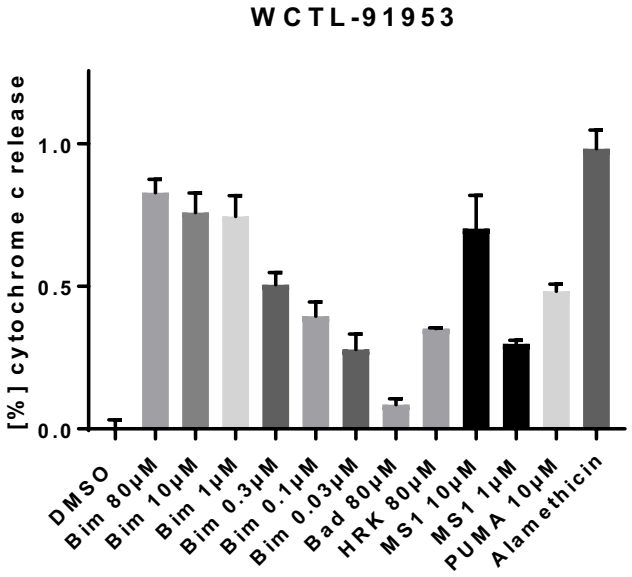

Figure 12. WCTL-91953 (Alk+ ALCL) is primarily MCL-1 dependent as determined by baseline BH3 profiling. This model undergoes significant cytochrome c release upon incubation with MS1 peptide (MCL-1 specific) but little cytochrome c release is seen from cells incubated with Bad (BCL-2 and BCL-XL) or HRK peptides (BCL-XL). DMSO: negative control. Alamethicin: positive control.

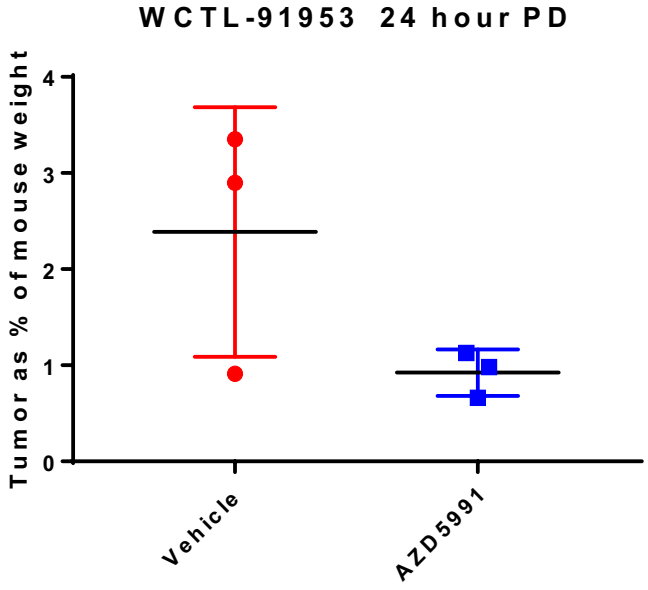

Figure 13. Tumor size as a percentage of body weight 24 hours after first dose of AZD5991 in WCTL-91953. P=0.127 by unpaired two-sided t-test.

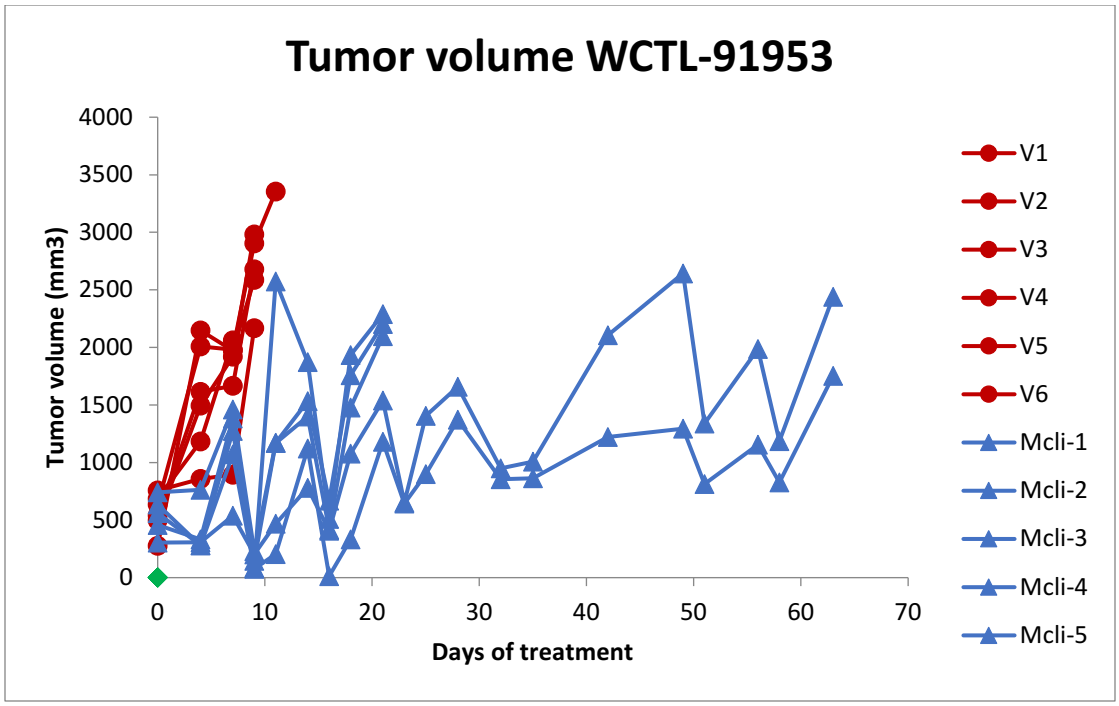

Figure 14. Tumor volume of WCTL-91953 individual mice.

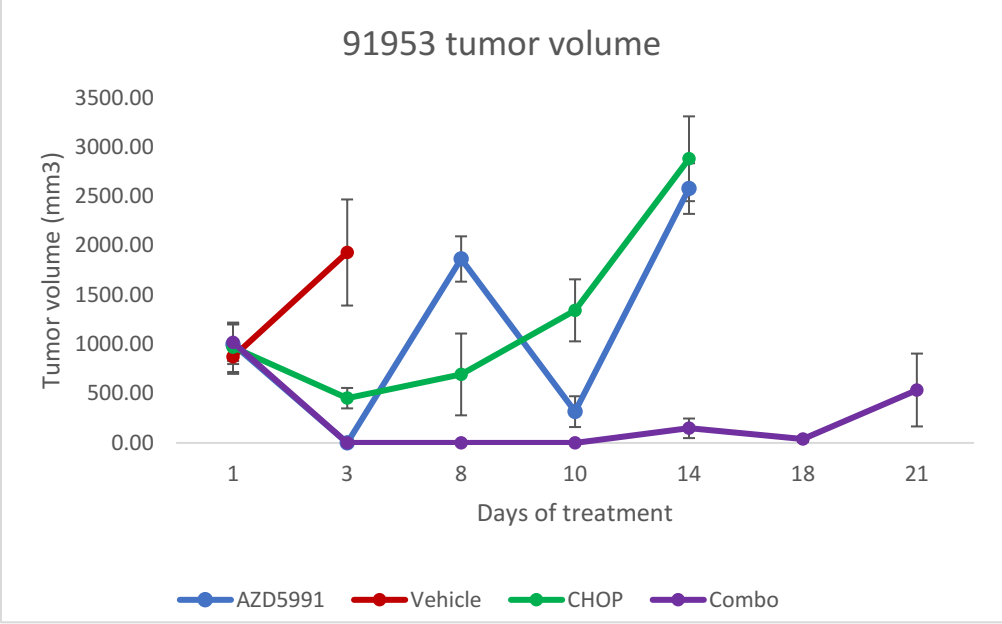

Figure 15. WCTL-91953 tumor volume for AZD5991 double dose and CHOP combination therapy (mean per arm).

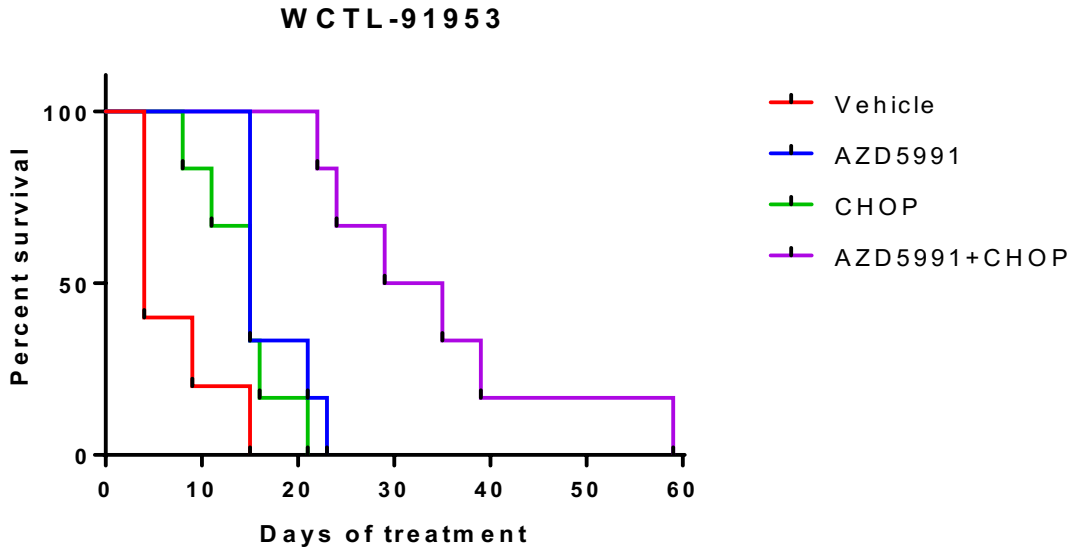

Figure 16. WCTL-91953 survival data for AZD5991 double dose and CHOP combination therapy.

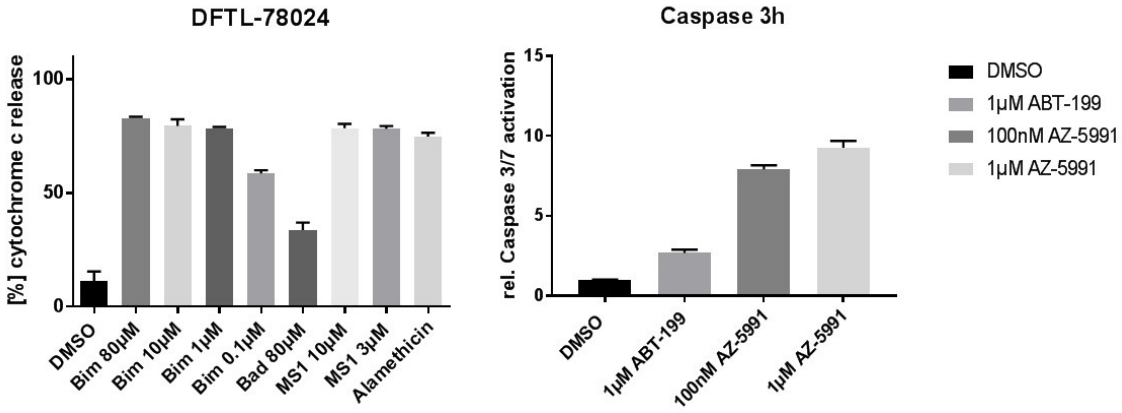

Figure 17. DFTL-78024 (AITL) has mixed dependency on MCL-1 and BCL-xL as determined by cytochrome c release after incubation with both MS1 and Bad peptides. Since Bad antagonizes both BCL-2 and BCL-XL, we performed a caspase 3/7 activation assay to identify sensitivity to the specific BCL-2 inhibitor ABT199. Treatment with ABT199 did not result in significant caspase activation which clarifies lack of dependence on BCL-2.

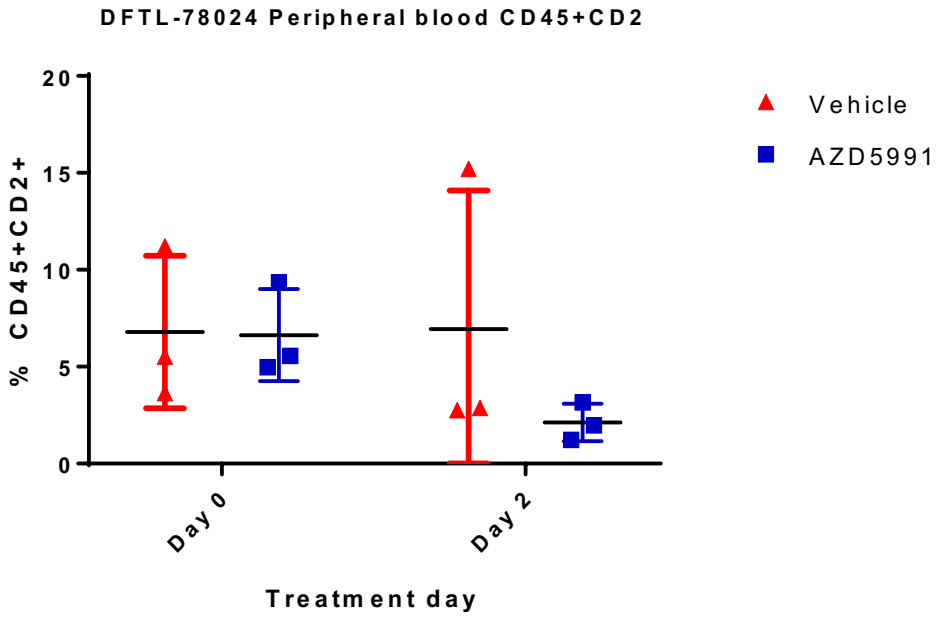

Figure 18. DFTL-78024 24-hour peripheral blood flow cytometry. P=0.311 (day 2) by unpaired two-sided t-test.

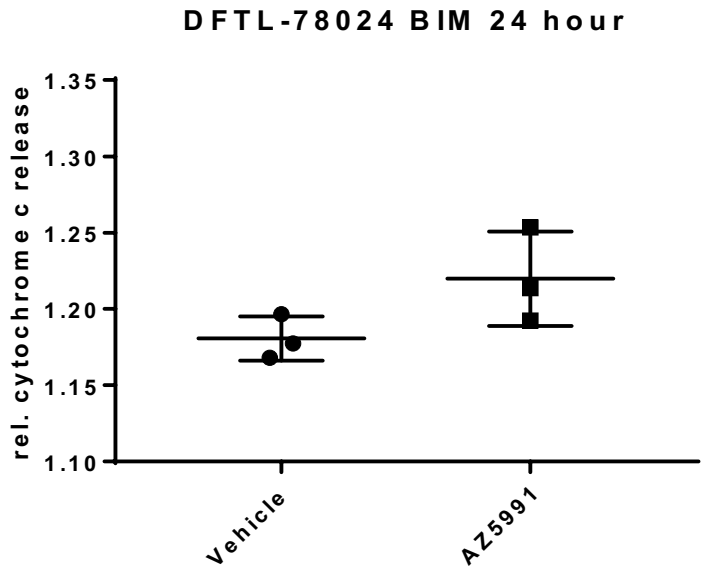

Figure 19. DFTL-78024 24-hour apoptosis induction by incubation with 0.3µM BIM. *In vivo* treatment with AZD5991 leads to a slight, but not statistically significant, increase in apoptotic priming (p=0.1179 by unpaired two-sided t-test).

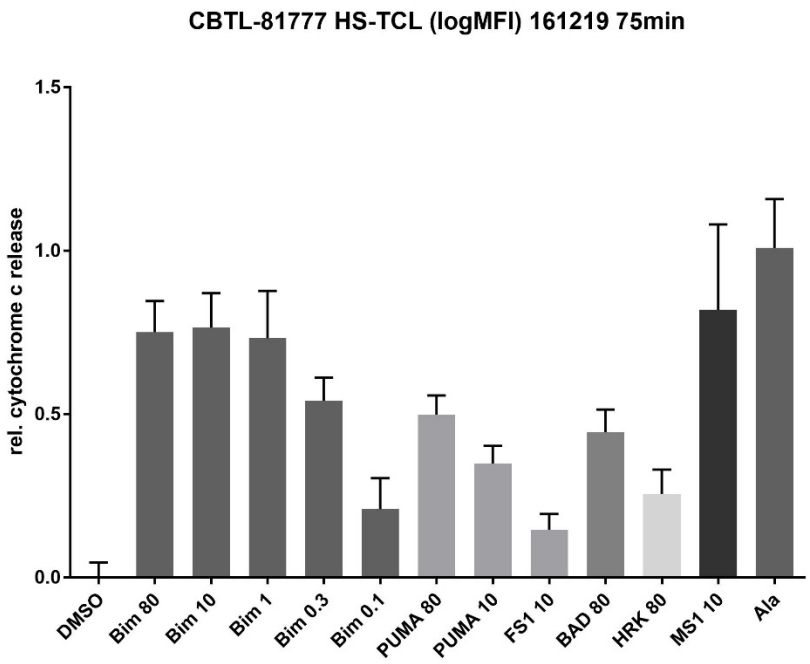

Figure 20. CBTL-81777 (HSCTL) has mixed dependency, with a primary MCL-1 dependence.

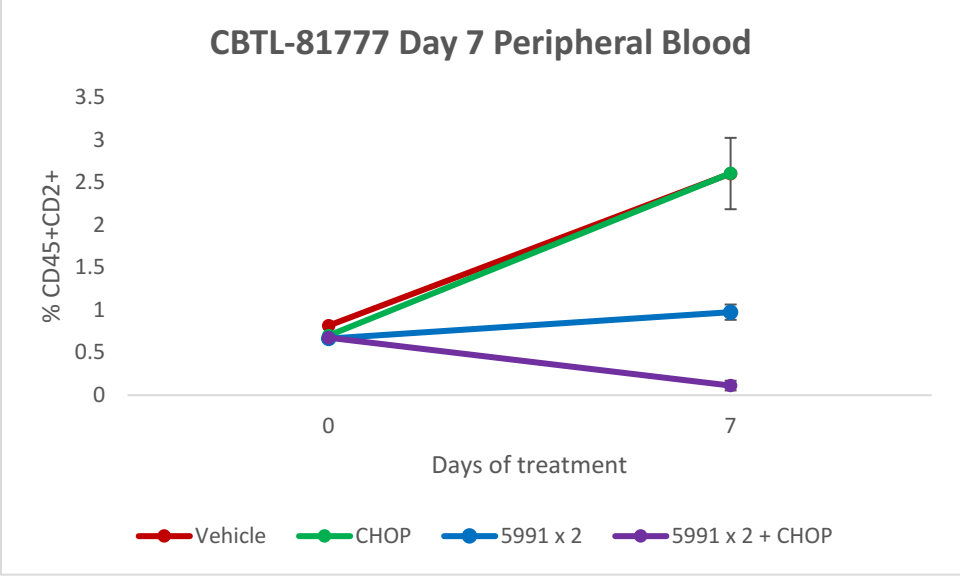

Figure 21. CBTL-81777 Day 7 peripheral blood disease burden.

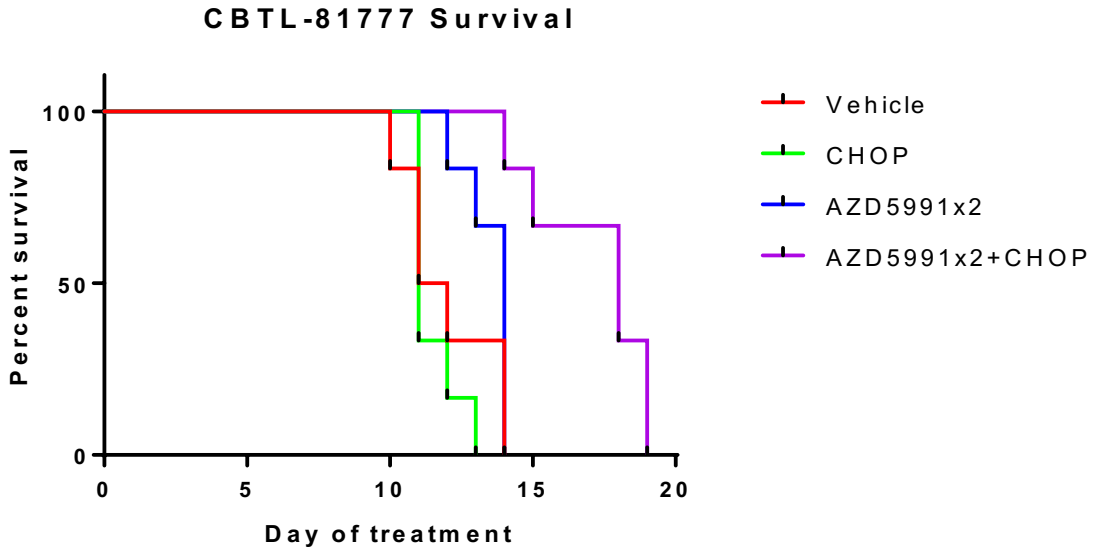

Figure 22. CBTL-81777 survival data.

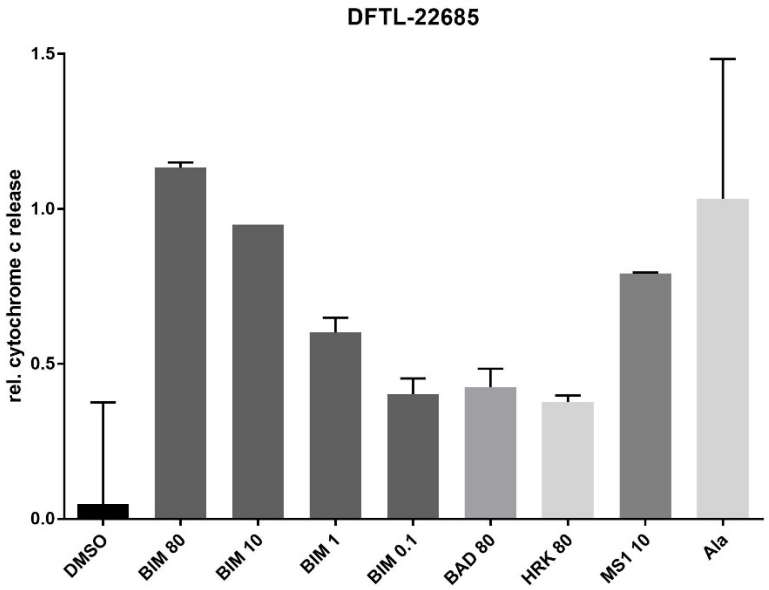

Figure 23. DFTL-22685 (CTCL) is primarily dependent on MCL-1.

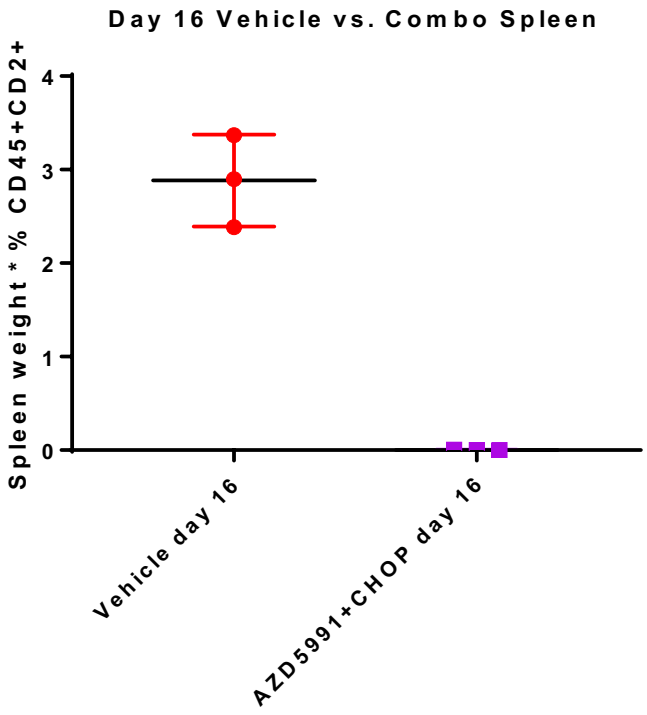

Figure 24. DFTL-22685 spleen disease normalized to spleen weight for mice sacrificed at day 16. P-value = 0.0005 by unpaired two-sided t-test.

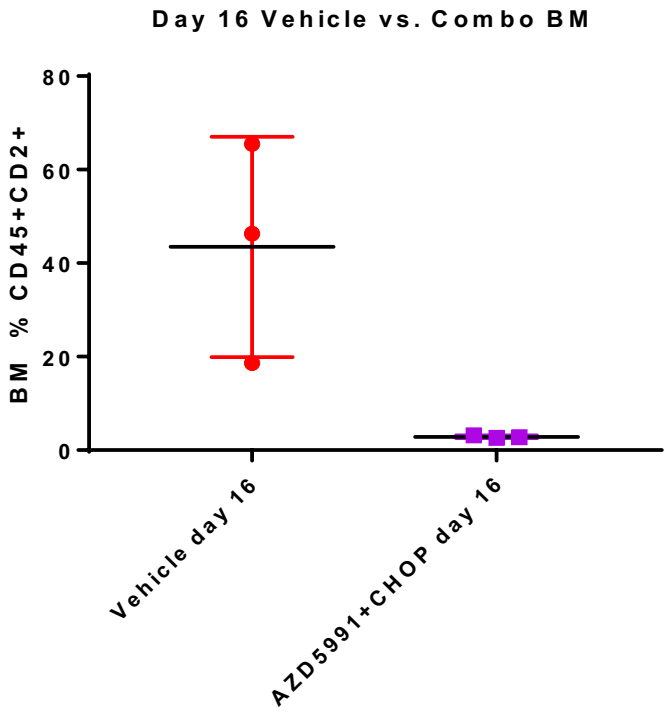

Figure 25. DFTL-22685 bone marrow disease for mice sacrificed at day 16. P-value = 0.0406 by unpaired two-sided t-test.

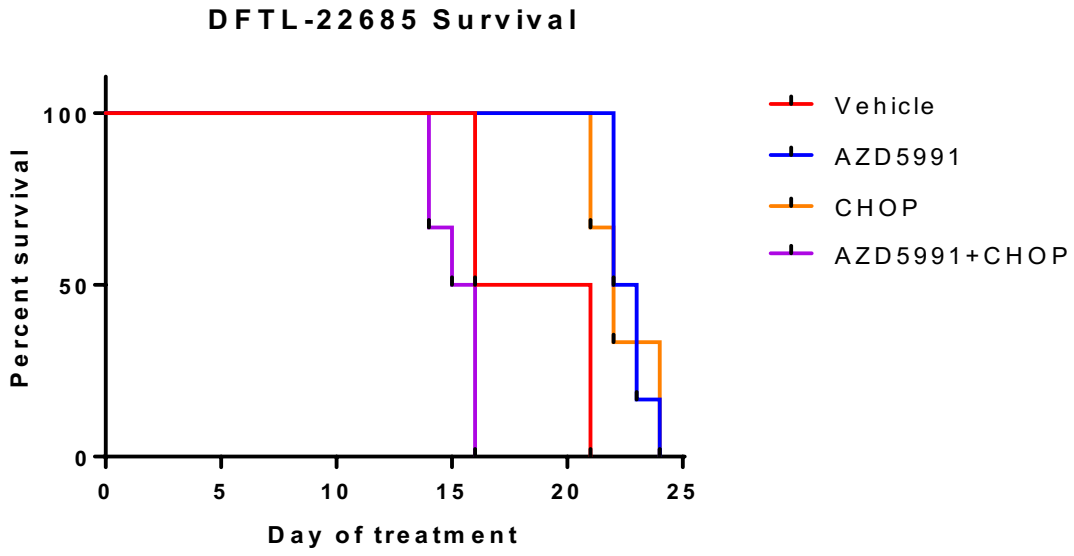

Figure 26. DFTL-22685 survival data.

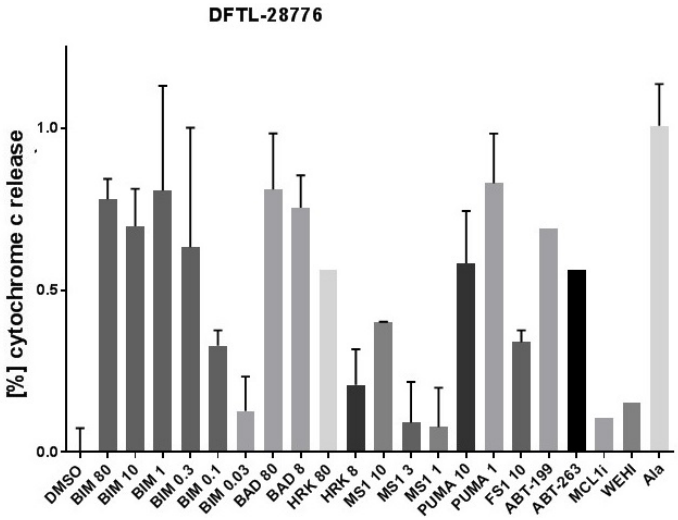

Figure 27. DFTL-28776 (T-PLL) is primarily dependent on BCL-XL as determined by high cytochrome c release after incubation with HRK peptide.

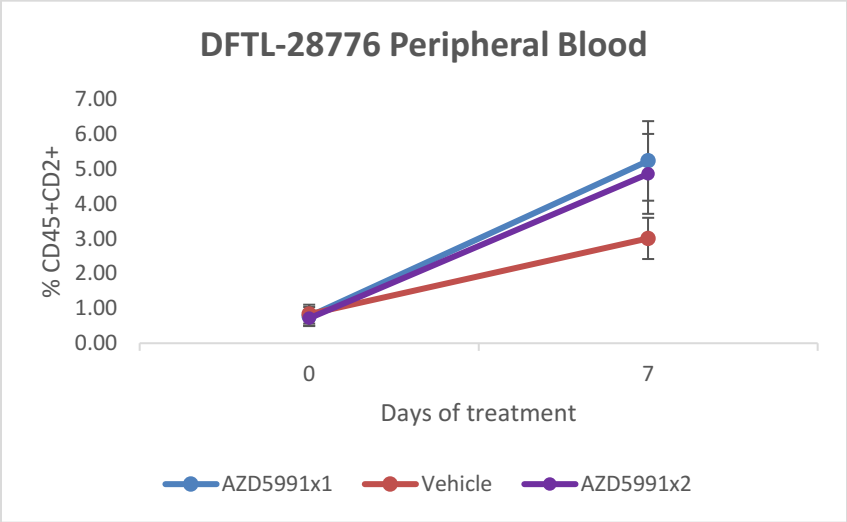

Figure 28. DFTL-28776 peripheral blood disease on day 7. There is no significant difference between groups by unpaired two-sided t-test.

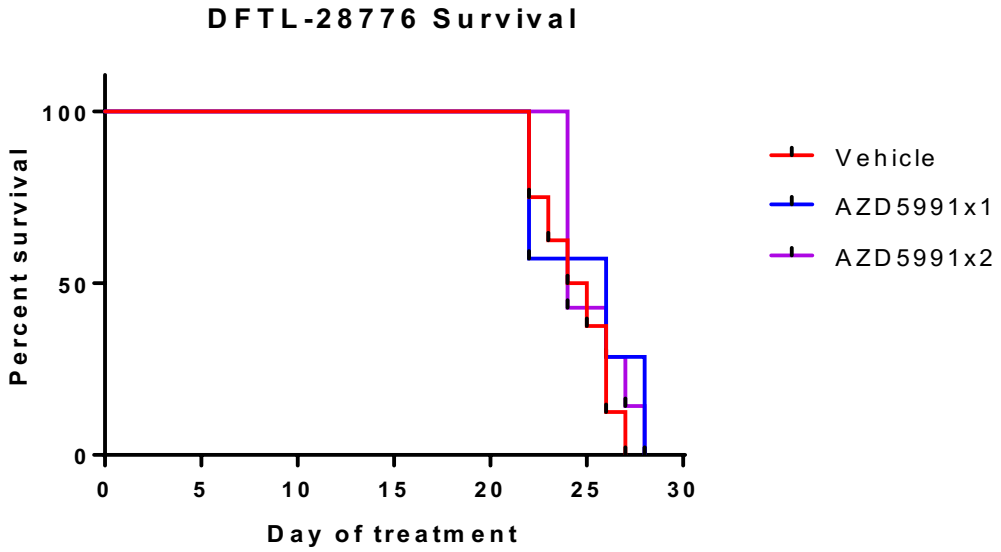

Figure 29. DFTL-28776 survival data.

References

Ashkenazi A, Fairbrother WJ, Leverson JD & Souers AJ. (2017). From basic apoptosis discoveries to advanced selective BCL-2 family inhibitors. *Nature Reviews Drug Discovery,* 16, 273-284.

Barretina J, Caponigro G, Stransky N, Venkatesan K, Margolin AA, Kim S, Wilson CJ, Lehar J, Kryukov GV, Sonkin D, Reddy A, Liu M, Murray L, Berger MF, Monahan JE, Morais P, Meltzer J, Korejwa A, Jane-Valbuena J, Mapa FA, Thibault J, Bric-Furlong E, Raman P, Shipway A, Engels IH, Cheng J, Yu GK, Yu J, Aspesi P, de Silva M, Jagtap K, Jones MD, Wang L, Hatton C, Palescandolo E, Gupta S, Mahan S, Sougnez C, Onofrio RC, Liefeld T, MacConaill L, Winckler W, Reich M, Li N, Mesirov JP, Gabriel SB, Getz G, Ardlie K, Chan V, Myer VE, Weber BL, Porter J, Warmuth M, Finan P, Harris JL, Meyerson M, Golub TR, Morrissey MP, Sellers WR, Schlegel R & Garraway LA. (2012). The Cancer Cell Line Encyclopedia enables predictive modeling of anticancer drug sensitivity. *Nature,* 483, 603-607.

Chonghaile TN, Roderick JE, Glenfield C, Ryan J, Sallan SE, Silverman LB, Loh ML, Hunger SP, Wood B, DeAngelo DJ, Stone R, Harris M, Gutierrez A, Kelliher MA & Letai A. (2014). Maturation stage of T-cell acute lymphoblastic leukemia determines BCL-2 versus BCL-xL dependence and sensitivity to ABT-199. *Cancer Discovery*, 4(9), 1074-1087.

Chowdry RP, Sica GL, Kim S, Chen Z, Goodman A, Alexis D, Deng X & Owonikoko TK. (2016). Phosphorylated BCL-2 and MCL-1 as prognostic markers in small cell lung cancer. *Oncotarget*, [epub ahead of print].

Daniel VC, Marchionni L, Hierman JS, Rhodes JT, Devereux WL, Rudin CM, Yung R, Parmigiani G, Dorsch M, Peacock CD & Watkins DN. (2009). A primary xenograft model of small-cell lung cancer reveals irreversible changes in gene expression imposed by culture *in vitro*. *Cancer Research,* 69(8), 3364-3373.

Fernández-Marrero Y, Spinner S, Kaufmann T & Jost PJ. (2016). Survival control of malignant lymphocytes by anti-apoptotic MCL-1. *Leukemia*, 30, 2152-2159.

Foss FM, Zinzani PL, Vose JM, Gascoyne RD, Rosen ST & Tobinai K. (2011). Peripheral T-cell lymphoma. *Blood,* 117(25), 6756-6767.

Gibson CJ and Davids MS. (2015). BCL-2 antagonism to target the intrinsic mitochondrial pathway of apoptosis. *Clinical Cancer Research*, 21(22), 5021-9.

Hanahan D & Weinberg RA. (2000). The hallmarks of cancer. *Cell*, 100(1), 57-70.

Hidalgo M, Amant F, Biankin AV, Budinská E, Byrne AT, Caldas C, Clarke RB, de Jong S, Jonkers J, Mælandsmo GM, Roman-Roman S, Seoane J, Trusolino L & Villanueva A. (2014). Patient-derived xenograft models: an emerging platform for translational cancer research. *Cancer Discovery*, 4, 998-1013.

Kotschy A, Szlavik Z, Murray J, Davidson J, Maragno AL, Le Toumelin-Braizat G, Chanrion M, Kelly GL, Gong JN, Moujalled DM, Bruno A, Csekei M, Paczal A, Szabo ZB, Sipos S, Radics G, Proszenyak A, Balint B, Ondi L, Blasko G, Robertson A, Surgenor A, Dokurno P, Chen I, Matassova N, Smith J, Pedder C, Graham C, Studeny A, Lysiak-Auvity G, Girard AM, Gravé F, Segal D, Riffkin CD, Pomilio G, Galbraith LC, Aubrey BJ, Brennan MS, Herold MJ, Chang C, Guasconi G, Cauquil N, Melchiore F, Guigal-Stephan N, Lockhart B, Colland F, Hickman JA, Roberts AW, Huang DC, Wei AH, Strasser A, Lessene G & Geneste O. (2016). The MCL1 inhibitor S63845 is tolerable and effective in diverse cancer models. *Nature*, 538(7626):477-482.

Lackner MR, Wilson TR & Settleman J. (2012). Mechanisms of acquired resistance to targeted cancer therapies. *Future Oncology,* 8(8), 999-1014.

Li HL, Huang XP, Zhou XH, Ji TH, Wu ZQ, Wang ZQ, Jiang HY, Liu FR & Zhao T. (2011). Correlation of seven biological factors (Hsp90α, p53, MDM2, Bcl-2, Bax, cytochrome c, and cleaved caspase 3) with clinical outcomes of ALK+ anaplastic large-cell lymphoma. *Biomedical Environmental Science*, 24(6), 630-641.

Lunning MA and Horowitz S. (2013). Treatment of peripheral T-cell lymphoma: are we data driven or driving the data? *Current Treatment Options in Oncology,* 14(2), 212-223.

Mak V, Hamm J, Chhanabhai M, Shenkier T, Klasa R, Sehn LH, Villa D, Gascoyne RD, Connors JM & Savage KJ. (2013). Survival of patients with peripheral T-cell lymphoma after first relapse or progression: spectrum of disease and rare long-term survivors. *Journal of Clinical Oncology*, 31(16), 1970-1976.

Montero J, Sarosiek KA, DeAngelo JD, Maertens O, Ryan J, Ercan D, Piao H, Horowitz NS, Berkowitz RS, Matulonis U, Janne PA, Amrein PC, Cichowski K, Drapkin R & Letai A. (2015). Drug-induced death signaling strategy rapidly predicts cancer response to chemotherapy. *Cell*, 160, 977-989.

Palve V, Mallick S, Ghaisas G, Kannan S & Teni T. (2014). Overexpression of MCL-1L splice variant is associated with poor prognosis and chemoresistance in oral cancers. *PLOS One*, 9(11).

Potter DS & Letai A. (2016). To prime, or not to prime: that is the question. *Cold Spring Harbor Laboratory on Quantitative Biology,* Volume LXXXI.

Rassidakis GZ, Jones D, Lai R, Ramalingam P, Sarris AH, McDonnell TJ & Medeiros LJ. (2003). BCL-2 family proteins in peripheral T-cell lymphomas: correlation with tumour apoptosis and proliferation. *Journal of Pathology*, 200, 240-248.

Ryan J, Montero J, Rocco J & Letai A. (2016). iBH3: simple, fixable BH3 profiling to determine apoptotic priming in primary tissue by flow cytometry. *Biological Chemistry*, 397(7), 671-678.

Sarosiek KA & Letai A. (2016). Directly targeting the mitochondrial pathway of apoptosis for cancer therapy using BH3 mimetics – recent successes, current challenges and future promise. *The FEBS Journal*, 283, 3523-3533.

Shigemasa K, Katoh O, Shiroyama Y, Mihara S, Mukai K, Nagai N & Ohama K. (2002). Increased MCL-1 expression is associated with poor prognosis in ovarian carcinomas. *Japanese Journal of Cancer Research,* 93, 542-550.

Spinner S, Crisoatzu G, Yi J-H, Mayer P, Höckendorf U, Müller N, Li Z, Schader T, Bendz H, Hartmann S, Yabai M, PechloffK, Heikenwalder M, Kelly GL, Strasser A, Peschel C, Hansmann M-L, Ruland J, Keller U, Newrzela S, Herling M & Jost PJ. (2016) Re-activation of mitochondrial apoptosis inhibits T-cell lymphoma survival and treatment resistance. *Leukemia*, 30, 1520-1530.

Swerdlow SH, Campo E, Pileri SA, Harris NL, Stein H, Siebert R, Advani R, Ghielmini M, Salles GA, Zelenetz AD & Jaffe ES. (2016). The 2016 revision of the World Health Organization classification of lymphoid neoplasms. *Blood*, 127(20), 2375-2390.

Townsend EC, Murakami MA, Christodoulou A, Christie AL, Koester J, DeSouza TA, Morgan EA, Kallgren SP, Liu H, Wu S-C, Plana O, Montero J, Stevenson KE, Andreeff M, Armand P, Ballen KK, Barzaghi-Rinaudo P, Cahill S, Clark RA, Cooke VG, Davids MS, DeAngelo DJ, Dorman DM, Eaton H, Ebert BL, Etchin J, Firestone B, Fisher DC, Freedman AS, Galinsky IA, Gao H, Garcia JS, Garnache-Ottou F, Graubert TA, Gutierrez A, Halilovic E, Harris MH, Herbert ZT, Horwitz SM, Inghirami G, Intlekofer AM, Ito M, Izraeli S, Jacobsen ED, Jacobson CA, Jeay S, Jeremias I, Kelliher MA, Koch R, Konopleva M, Kopp N, Kornblau SM, Kung AL, Kupper TS, LeBoeuf N, LaCasce AS, Lees E, Li L, Look AT, Murakami M, Muschen M, Neuberg D, Ng SY, Odejide OO, Orkin SH, Paquette RR, Place AE, Roderick JE, Ryan JA, Sallan SE, Shoji B, Silverman LB, Soiffer RJ, Steensma DP, Stegmaier K, Stone RM, Tamburini J, Thorner AR, van Hummelen P, Wadleigh M, Wiesmann M, Weng AP, Wuerthner JU, Williams DA, Wollison BM, Lane AA, Letai A, Bertagnolli M, Ritz J, Brown M, Long H, Aster JC, Shipp M, Griffin JD, Weinstock DM. (2016). The Public Repository of Xenografts (PRoXe) enables discovery and randomized phase II-like trials in mice. *Cancer Cell*, 29(4), 574-586.

Weigert O, Lane AA, Bird L, Kopp N, Chapuy B, van Bodegom D, Toms AV, Marubayaski S, Christie AL, McKeown M, Paranal RM, Bradner JE, Yoda A, Gaul C, Vangrevelinghe E, Romanet V, Murakami M, Tiedt R, Ebel N, Evrot E, De Pover A, Regnier CH, Erdmann D, Hofmann F, Eck MJ, Sallan SE, Levine RL, Kung AL, Baffert F, Radimerski T, Weinstock DM. (2012). Genetic resistance to JAK2 enzymatic inhibitors is overcome by HSP90 inhibition. *The Journal of Experimental Medicine*, 209(2), 259-273.

Wunderlich M, Mizukawa B, Chou F-S, Sexton C, Shrestha M, Saunthawrarajah Y, Mulloy JC. (2013). AML cells are differentially sensitive to chemotherapy treatment in a human xenograft model. *Blood*, 121(12), e90-97.

Yoda A, Adelmant G, Tamburini J, Chapuy B, Shindoh N, Yoda Y, Weigert O, Kopp N, Wu SC, Kim SS, Liu H, Tivey T, Christie AL, Elpek KG, Card J, Gritsman K, Gotlib J, Deininger MW, Makishima H, Turley SJ, Javidi-Sharifi N, Maciejewski JP, Jaiswal S, Ebert BL, Rodig SJ, Tyner JW, Marto JA, Weinstock DM & Lane AA. (2015). Mutations in G protein β subunits promote transformation and kinase inhibitor resistance. *Nature Medicine*, 21(1), 71-75.

Zhang Y, Xu W, Liu H & Li J. (2016). Therapeutic options in peripheral T-cell lymphoma. *Journal of Hematology & Oncology*, 9(37).